AP-1 and KIF13A coordinate endosomal sorting and positioning during melanosome biogenesis

Cédric Delevoye,[1,4] Ilse Hurbain,[1,2,4] Danièle Tenza,[1,2,4] Jean-Baptiste Sibarita,[2,4] Stéphanie Uzan-Gafsou,[3,4] Hiroshi Ohno,[5] Willie J.C. Geerts,[6] Arie J. Verkleij,[6] Jean Salamero,[2,3,4] Michael S. Marks,[7] and Graça Raposo[1,2,4]

[1]Structure and Membrane Compartments, [2]Cell and Tissue Imaging Facility (IBiSA), [3]Molecular Mechanisms of Intracellular Transport, and [4]Centre Nationale de la Recherche Scientifique, UMR 144 Institut Curie, Centre de Recherche, Paris F-75248, France
[5]Research Center for Allergy and Immunology, RIKEN, Yokohama, Kanagawa 230-0045, Japan
[6]Department of Cellular Architecture and Dynamics, Universiteit Utrecht, Utrecht 3584 CH, Netherlands
[7]Department of Pathology and Laboratory Medicine, University of Pennsylvania, Philadelphia, PA 19104

Specialized cell types exploit endosomal trafficking to deliver protein cargoes to cell type–specific lysosome-related organelles (LROs), but how endosomes are specified for this function is not known. In this study, we show that the clathrin adaptor AP-1 and the kinesin motor KIF13A together create peripheral recycling endosomal subdomains in melanocytes required for cargo delivery to maturing melanosomes. In cells depleted of AP-1 or KIF13A, a subpopulation of recycling endosomes redistributes to pericentriolar clusters, resulting in sequestration of melanosomal enzymes like Tyrp1 in vacuolar endosomes and consequent inhibition of melanin synthesis and melanosome maturation. Immunocytochemistry, live cell imaging, and electron tomography reveal AP-1– and KIF13A-dependent dynamic close appositions and continuities between peripheral endosomal tubules and melanosomes. Our results reveal that LRO protein sorting is coupled to cell type–specific positioning of endosomes that facilitate endosome–LRO contacts and are required for organelle maturation.

Introduction

The endosomal system is a complex network of organelles and membrane subdomains with essential roles in eukaryotic cells for physiological processes such as nutrient uptake, macromolecule degradation, and signaling. The early endosomal network, comprising sorting and recycling endosomes, consists of vacuolar and tubulovesicular domains that promote trafficking to and from the cell surface or toward lysosomes or the TGN (Gould and Lippincott-Schwartz, 2009). Within endosomes, transmembrane cargoes are sorted into tubulovesicular intermediates bound for distinct destinations by interactions of cytoplasmic-sorting signals with coat and coat-like protein complexes, including the adaptors AP-1, -2, -3, and -4 (Bonifacino and Glick, 2004). To effect cargo delivery toward target organelles, cargo sorting must be tied to membrane motility, as cytoskeletal dynamics regulate the positioning of endosomes and the formation and target delivery of vesicles and tubules (Soldati and Schliwa, 2006). Interactions between Rab GTPases and molecular motors coordinate organelle positioning (Stenmark, 2009), but how cargo sorting is coupled to vesicle/tubule motility toward target membranes is not understood.

In most well-studied cells, the ability to link cargo sorting to organelle positioning and carrier motility is complicated by the redundancy of sorting pathways from early endosomes toward lysosomes or the TGN. In contrast, some specialized cells harbor specialized organelles in which some of these pathways are essential for effective cargo delivery. These cells provide a unique model system to dissect mechanisms associated with a single early endosome–derived transport step. For example, lysosome-related organelles (LROs) are cell type–specific compartments that arise by delivery of specific cargoes from early endosomal intermediates (for review see Raposo and Marks, 2007). Melanosomes, the pigment granules of skin and eye melanocytes and eye pigment epithelial cells, represent a class of

Correspondence to Graça Raposo: graposo@curie.fr

J.-B. Sibarita's present address is Université Bordeaux, Institut François Magendie, Bordeaux 33077, France

Abbreviations used in this paper: CCD, charge-coupled device; HPF, high pressure freezing; HPS, Hermansky–Pudlak syndrome; IB, incubation buffer; IEM, immuno-EM; IFM, immunofluorescence microscopy; LRO, lysosome-related organelle; Tf, transferrin.

The Rockefeller University Press $30.00
J. Cell Biol. Vol. 187 No. 2 247–264
www.jcb.org/cgi/doi/10.1083/jcb.200907122

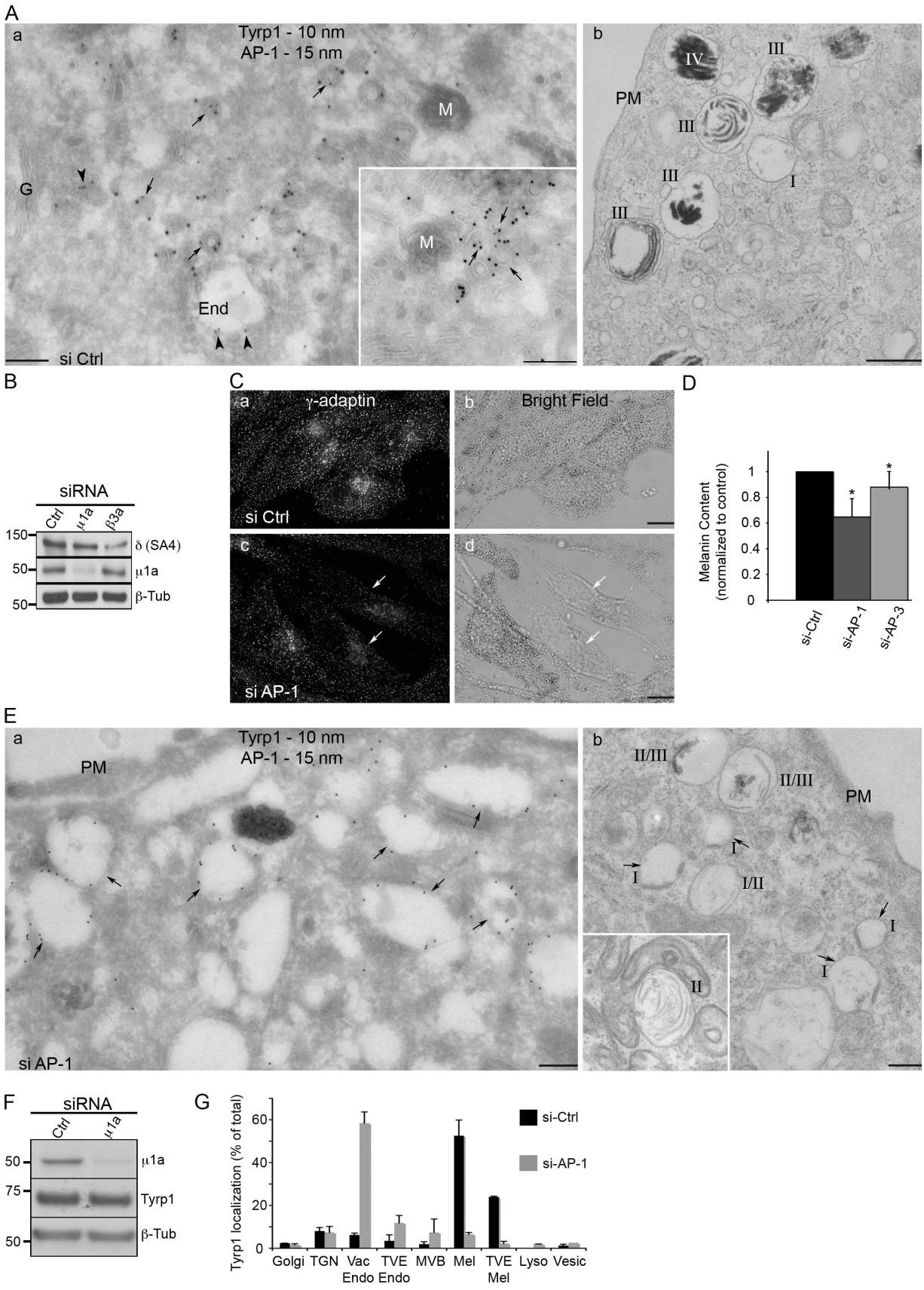

Figure 1. **Depletion of AP-1 inhibits melanogenesis and results in Tyrp1 accumulation in endosomal vacuoles.** (A) MNT-1 cells treated with control siRNA (si Ctrl) were analyzed by ultracryomicrotomy (a) or conventional EM (b). (a) In control-inactivated cells, Tyrp1 is detected in vesicles close to the Golgi apparatus in vacuolar endosomes (arrowheads) and in AP-1–positive vesicles and tubules in the vicinity of endosomes (arrows) and pigmented melanosomes

LROs that segregate from the conventional endocytic pathway and coexist with late endosomes and lysosomes. Specialized pathways divert cargoes from conventional compartments toward melanosomes (for review see Raposo and Marks, 2007), making these organelles an excellent model system to define how protein sorting and endosome motility are linked.

Melanosomes mature through four distinct morphological stages (Seiji et al., 1963), beginning with the transformation of vacuolar endosome intermediates (stage I) into nonpigmented stage II premelanosomes bearing intralumenal fibrillar sheets (Hurbain et al., 2008) upon which melanin ultimately deposits. Melanin synthesis in late-stage (III and IV) melanosomes requires the selective targeting of integral membrane melanogenic enzymes, such as tyrosinase and Tyrp1 (tyrosinase-related protein 1), and other components that regulate enzyme activity, from early endosomal intermediates to stage II melanosomes (for review see Raposo and Marks, 2007). Among the machinery that regulates cargo delivery to maturing melanosomes are the products of genes that are mutated in Hermansky–Pudlak syndrome (HPS), a group of multisystem genetic disorders of LRO formation characterized by hypopigmentation and other systemic defects (Wei, 2006; Huizing et al., 2008). Most of the genes that are defective in HPS encode subunits of four ubiquitously expressed cytoplasmic multisubunit complexes, the adaptor AP-3 and BLOC-1 (biogenesis of LRO complex 1), -2, and -3 (Dell'Angelica, 2004). Studies in melanocytes from HPS patients and their mouse models revealed that cargoes destined for melanosomes emerge from distinct domains on early endosomes by at least two pathways that require AP-3 and BLOC-1/BLOC-2, respectively (Huizing et al., 2001; Helip-Wooley et al., 2005; Theos et al., 2005; Di Pietro et al., 2006; Setty et al., 2007, 2008). However, neither the nature of the endosomal subdomains from which these complexes function nor the precise role for other effectors within these pathways has yet been established.

Among additional suspected effectors of melanosomal enzyme trafficking, the adaptor AP-1 is thought to function in an alternative pathway to the one regulated by AP-3, permitting pigmentation of AP-3–deficient cells (Theos et al., 2005). Like AP-3, AP-1 binds in vitro to cytoplasmic targeting signals on tyrosinase and OCA2 (Theos et al., 2005; Chapuy et al., 2008; Sitaram et al., 2009). Moreover, AP-1 uniquely binds to a targeting signal on Tyrp1 (Theos et al., 2005) and is detected in melanocytic cells on coated vesicles and buds that are enriched in tyrosinase and Tyrp1 (Raposo et al., 2001; Theos et al., 2005). This suggested that AP-1 functions in melanosomal cargo delivery. In addition, the detection of many AP-1– and AP-3–coated buds near melanosomes (Theos et al., 2005) led us to hypothesize that LRO-containing cells exploit specialized mechanisms not only for vesicle formation and targeting but also for the maintenance and positioning of endosomal domains to ensure efficient cargo transfer to LROs. If cargo sorting were functionally linked to endosomal positioning, adaptors might play a key role in both processes.

Using gene silencing and imaging approaches, we show that AP-1 is required for trafficking of at least one cargo, Tyrp1, from endosomes to maturing melanosomes. The endosomal sorting function of AP-1 requires its interaction with the microtubule plus end–directed motor KIF13A. Importantly, this requirement correlates with a function for AP-1 and KIF13A in creating, maintaining, and positioning subdomains of the recycling endosomal system, which establish direct continuities with maturing melanosomes. Our findings show how a coat protein and a microtubule motor coordinately regulate endosomal sorting and endosome positioning to facilitate interorganellar cross talks essential for organelle biogenesis.

Results

Functional AP-1 is required for melanosomal cargo exit from endosomes

The cytoplasmic domain of Tyrp1 binds in vitro to AP-1 (Theos et al., 2005), and Tyrp1 coimmunoprecipitates with AP-1 in vivo (see Fig. 5 E). Moreover, a cohort of Tyrp1 is localized at steady state in endosomes (Fig. 1 A, arrowheads) and in AP-1–coated vesicles and tubules (Fig. 1 A, arrows), many of which are detected within 0.5 µm of melanosomes (Raposo et al., 2001). These compartments likely represent intermediates in the biosynthetic delivery of Tyrp1 from endosomes to forming stage III/IV melanosomes (Fig. 1 A, b). To test whether AP-1 is required for melanogenic protein delivery to melanosomes, we analyzed pigmentation and Tyrp1 localization in melanocytic MNT-1 cells depleted of AP-1. Treatment of MNT-1 cells with siRNAs targeting µ1A (Fig. 1 B) decreases expression of the indicated AP-1 subunit by 80 ± 7%. Relative to control cells, melanin content in AP-1–depleted cells is reduced by >40% (Fig. 1, C and D). In contrast, inactivation of the related AP-3 complex, which mediates melanosomal delivery of a cohort of tyrosinase, decreases melanin content by only 20% (Fig. 1 D), paralleling the substantial pigmentation of AP-3–deficient mouse melanocytes (Theos

(inset, arrows). (b) Control cells show different melanosomal stages including unpigmented (stage I) and pigmented melanosomes (stages III and IV). G, Golgi apparatus; M, melanosome; PM, plasma membrane; End, endosome; I–IV, stages I–IV. (B) Western blot analysis of lysates of MNT-1 cells treated with control, AP-1 (µ1A), and AP-3 (β3A) siRNAs using SA4 (δ subunit of AP-3), anti-µ1A, or anti–β-tubulin antibodies as a loading control. (C) MNT-1 cells treated with control (a and b) or µ1A/γ-adaptin (c and d) siRNAs were labeled for AP-1 (γ-adaptin subunit) and observed by IFM (a and c) and bright field microscopy (b and d). Note the decrease of pigmented melanosomes in AP-1–depleted cells (arrows). (D) Evaluation of melanin content of cells treated with control, AP-1 (µ1A), or AP-3 (β3A) siRNAs. Data represent four replicates ± SD; *, $P < 0.05$. (E) Cells treated with AP-1 siRNAs were analyzed as described in A. (a) In inactivated cells, the bulk of Tyrp1 localizes to vacuolar endosomes (arrows). (b) Pigmented melanosomes are barely observed in AP-1–depleted cells. These cells accumulate vacuolar endosomes often displaying cytosolic coats (arrows). Characteristic stage II premelanosomes are observed in AP-1–depleted cells (b, inset). (F) Western blot analysis of lysates of MNT-1 cells treated with control or AP-1 siRNAs using anti-µ1A, Tyrp1, or anti–β-tubulin antibodies as a loading control. (G) Quantification of immunogold labeling for Tyrp1 on ultrathin cryosections. Localization of an equivalent number of gold particles in each sample was assessed relative to the indicated cell compartments. Data are presented as mean ± SD. Vac Endo, vacuolar endosome; TVE Endo, tubulovesicular endosomes associated to endosomes; MVB, multivesicular body; Mel, melanosome; TVE Mel, tubulovesicular endosomes associated to melanosomes; Lyso, lysosome; Vesic, vesicle. (B and F) Molecular masses are given in kilodaltons. Bars: (A and E) 200 nm; (C) 10 µm.

et al., 2005). These numbers likely underestimate the requirement for AP-1 and -3 in new pigmentation because they include melanosomes premade before siRNA treatment. To test whether AP-1 influences melanosomal enzyme trafficking and melanosome maturation, we assessed Tyrp1 localization upon AP-1 depletion by immuno-EM (IEM; Fig. 1 E, a) and analyzed melanosome morphology by conventional EM (Fig. 1 E, b). AP-1–deficient cells show a reduced number of mature melanosomes and an accumulation of vacuolar compartments with morphological features of endosomes (electron-lucent vacuoles with few intraluminal vesicles and cytosolic coats) where Tyrp1 accumulates (Fig. 1 E, arrows). Unpigmented stage II premelanosomes are still observed (Fig. 1 E, inset), indicating that AP-1 is not required for their formation. Together, these data indicate that AP-1 is required for maturation of stage III/IV melanosomes. Tyrp1 expression levels, determined by immunoblotting, are not consistently altered in AP-1–deficient cells relative to controls (Fig. 1 F), indicating that reduced melanogenesis does not reflect melanogenic enzyme degradation or cellular dedifferentiation. Quantitative analysis of immunogold labeling on ultrathin cryosections shows that Tyrp1 localization is dramatically altered by AP-1 deficiency (Fig. 1 G). Although Tyrp1 in control cells localizes primarily to melanosomes (53 ± 7%) and tubulovesicular endosomes in proximity to melanosomes (24 ± 0.2%), Tyrp1 in AP-1–deficient cells accumulates instead in vacuolar endosomes (58 ± 5%; Fig. 1 E, a, arrows). These data indicate that in the absence of AP-1, sorting of Tyrp1, and likely of other cargoes required for pigmentation, from endosomes and consequent melanosome maturation are impaired. The results imply that AP-1 functions in the selective removal of melanosomal cargoes from endosomes into carriers destined for maturing melanosomes.

AP-1 functions from peripheral recycling endosome subdomains that are apposed to maturing melanosomes

We next sought to characterize the endosomal compartments from which AP-1 functions in melanocytic cells. By immunofluorescence microscopy (IFM), AP-1 is distributed in punctate structures throughout MNT-1 cells (Fig. 2 A, b, f, and j) and is not highly enriched in the Golgi/perinuclear area, as is observed in other cell types (Waguri et al., 2003). AP-1 in these cells represents the ubiquitous AP-1A isoform and not AP-1B, which functions in polarized sorting to the basolateral cell surface of epithelial cells (Fölsch et al., 2001) because RT-PCR analysis shows that MNT-1 cells express only the μ1A subunit of AP-1 and not μ1B (Fig. S2 B) as previously reported (Valencia et al., 2006).

To identify the compartment with which AP-1 associates, γ-adaptin was localized relative to early sorting or recycling endosomes labeled by transferrin (Tf) conjugated to Alexa Fluor 488 (Tf-A488) that was internalized for various times or by antibodies to Rab11 (recycling endosomes; Ullrich et al., 1996) and EEA1 (sorting endosomes; Simonsen et al., 1998). Tf-A488 that was internalized constantly for 45 min labeled primarily recycling endosomal domains because it partially codistributed with Rab11 (Fig. S1 B, arrows) but not with EEA1, LAMP-1, or TGN46 (Fig. S1, A, C, and D, respectively). Although not fully overlapping, most of the AP-1 signal, like that of Rab11, was adjacent to Tf-loaded compartments after 45 min of internalization (Fig. 2, A [a–d, arrows] and B [quantification]) or pulsed for 10 min followed by 30 min of chase (not depicted). Consistently, the AP-1–containing puncta also abut Rab11-labeled structures (Fig. 2, A [h, arrows] and B; Ullrich et al., 1996) but not EEA1-labeled structures (Fig. 2 A, i–l). These observations indicate that AP-1 localizes to peripherally distributed subdomains of recycling endosomes.

The peripheral distribution of contiguous AP-1–, Rab11-, and Tf-containing recycling endosomal domains in pigmented melanocytic cells contrasts with classical recycling endosomes that concentrate in the pericentriolar region in other cell types (Hopkins et al., 1994), although it resembles the peripheral recycling endosome network in macrophages (Cox et al., 2000). Intriguingly, these recycling endosomal domains are often detected adjacent to Tyrp1-containing melanosomes (Fig. S1 F, arrowheads) but not to Pmel17-containing early-stage melanosomes or LAMP-1–containing late endosomes/lysosomes (Fig. S1, C and E). Consistently, IEM analyses show that the tubules that are most closely apposed to melanosomes are filled with Tf-biotin conjugates (Tf-biot) only after 45 min of internalization (Fig. 2 C). Many of these tubules bear AP-1 buds (Fig. 2 C, b, arrows) and are distinct from EEA1-labeled tubules and vacuoles (Fig. S2 A, black star) that are filled by Tf-biot after 10 min of internalization (Fig. S2 A, a and b). Moreover, some 45-min Tf-biot–labeled endosomal tubules contact and even surround mature, pigmented melanosomes (Fig. 2 C, a, arrows) but not Pmel17-containing early-stage melanosomes (Fig. S2 A, white star). These data show that AP-1 resides on peripheral tubulovesicular domains of recycling endosomes that are specifically apposed to mature melanosomes.

Because AP-1 is required for Tyrp1 transport from endosomes to melanosomes, we hypothesized that the peripheral recycling endosomal AP-1/Tf–containing domains are conduits for melanosomal delivery of Tyrp1. If correct, a cohort of Tyrp1 in transit should be detected in them. Although low resolution impedes detection of these intermediates by IFM (Fig. S1 F), qualitative and quantitative evaluation by IEM reveals that a significant fraction (24 ± 0.2%) of Tyrp1 localizes to endosomal intermediates and AP-1–coated vesicles near melanosomes (Fig. 1, A [a] and G). Consistently, the Tf-biot–filled tubules that are apposed to melanosomes are labeled for Tyrp1 (Fig. 2 C, c and d, arrows) but not for the early-stage melanosomal protein Pmel17 (Fig. S2 A, d). These results support the hypothesis that the peripherally distributed recycling endosomes function in biosynthetic cargo delivery to maturing melanosomes. Moreover, they suggest that specialized cells exploit peripheral positioning of recycling endosomal domains to divert cargoes toward tissue-specific LROs.

AP-1 is required for the peripheral distribution of recycling endosome subdomains

To test whether AP-1 plays a role in establishing the unusual peripheral distribution of recycling endosome subdomains and the endosome–melanosome network, we analyzed endosome positioning in MNT-1 cells that were depleted of AP-1A by

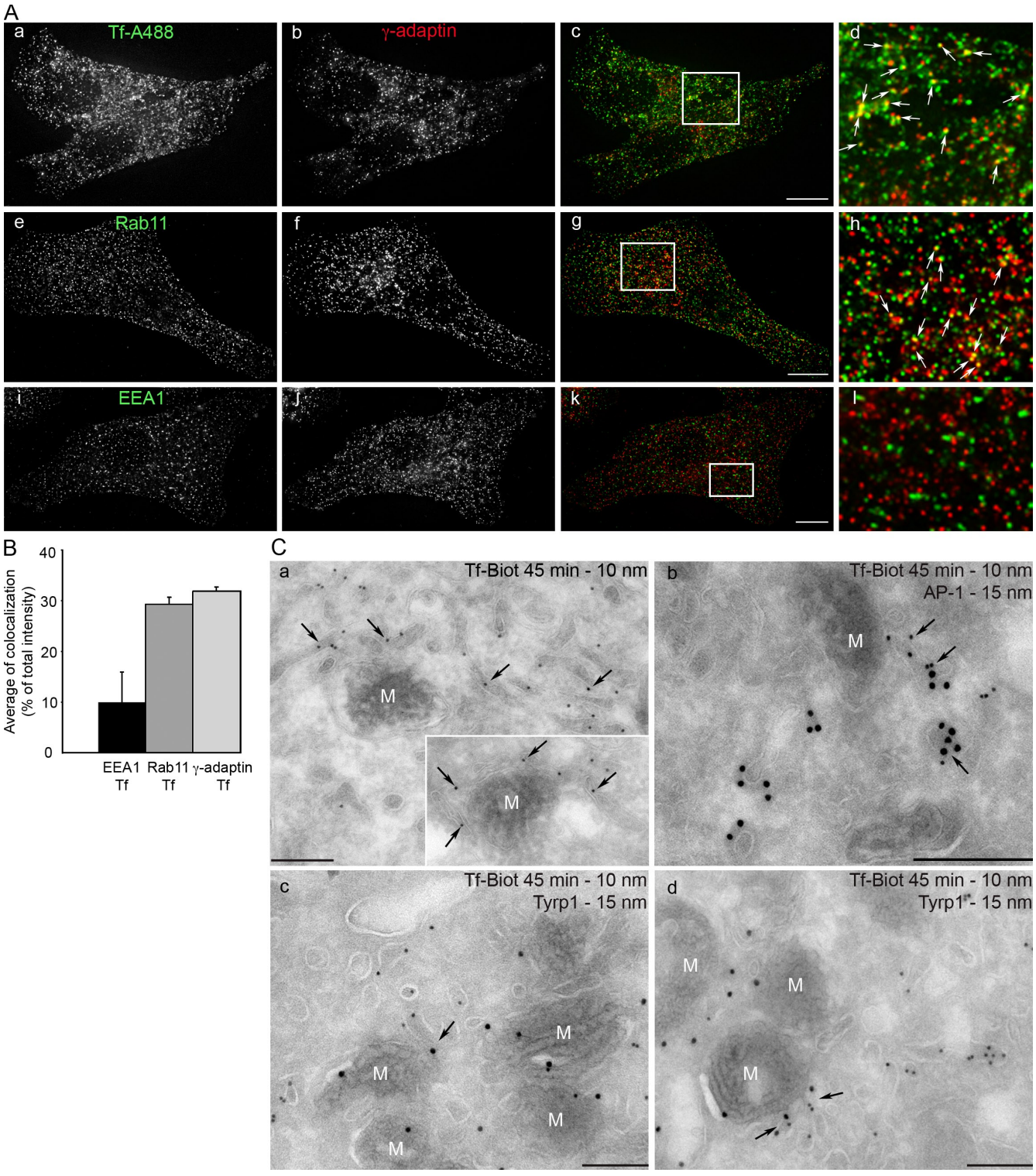

Figure 2. **AP-1 and Tyrp1 localize to subdomains of the recycling compartment adjacent to melanosomes.** (A) MNT-1 cells that had internalized Tf-A488 for 45 min were analyzed by IFM after labeling for AP-1 (γ-adaptin; a–d), Rab11 (e–h), or EEA1 (i–l). Single labeling is shown in columns 1 and 2, merged images in 3, and magnified insets (of boxed areas) in 4. Note that AP-1 partially overlaps with Tf-A488 (a–d, arrows) and Rab11 (e–h, arrows) but not with EEA1 (i–l). (B) Quantification of colocalization between Tf and EEA1, Rab11, or γ-adaptin in IFM experiments as described in A. Data are presented as mean ± SD. (C) MNT-1 cells that had internalized Tf-biot for 45 min were processed for ultrathin cryosectioning and single immunogold labeled for biotin (PAG10; a) or double immunogold labeled for biotin (PAG10) and γ-adaptin (PAG15; b) or for Tyrp1 (PAG 15; c and d). After 45 min of internalization, Tf-biot localizes to a tubular network that is close to and surrounds melanosomes (a and inset, arrows). These Tf-positive tubules often bear AP-1 buds (b, arrows). Tyrp1 is present on the limiting membrane of pigmented melanosomes (M) and is also detected on the Tf-positive tubules (c and d, arrows). Bars: (A) 10 μm; (C) 200 nm.

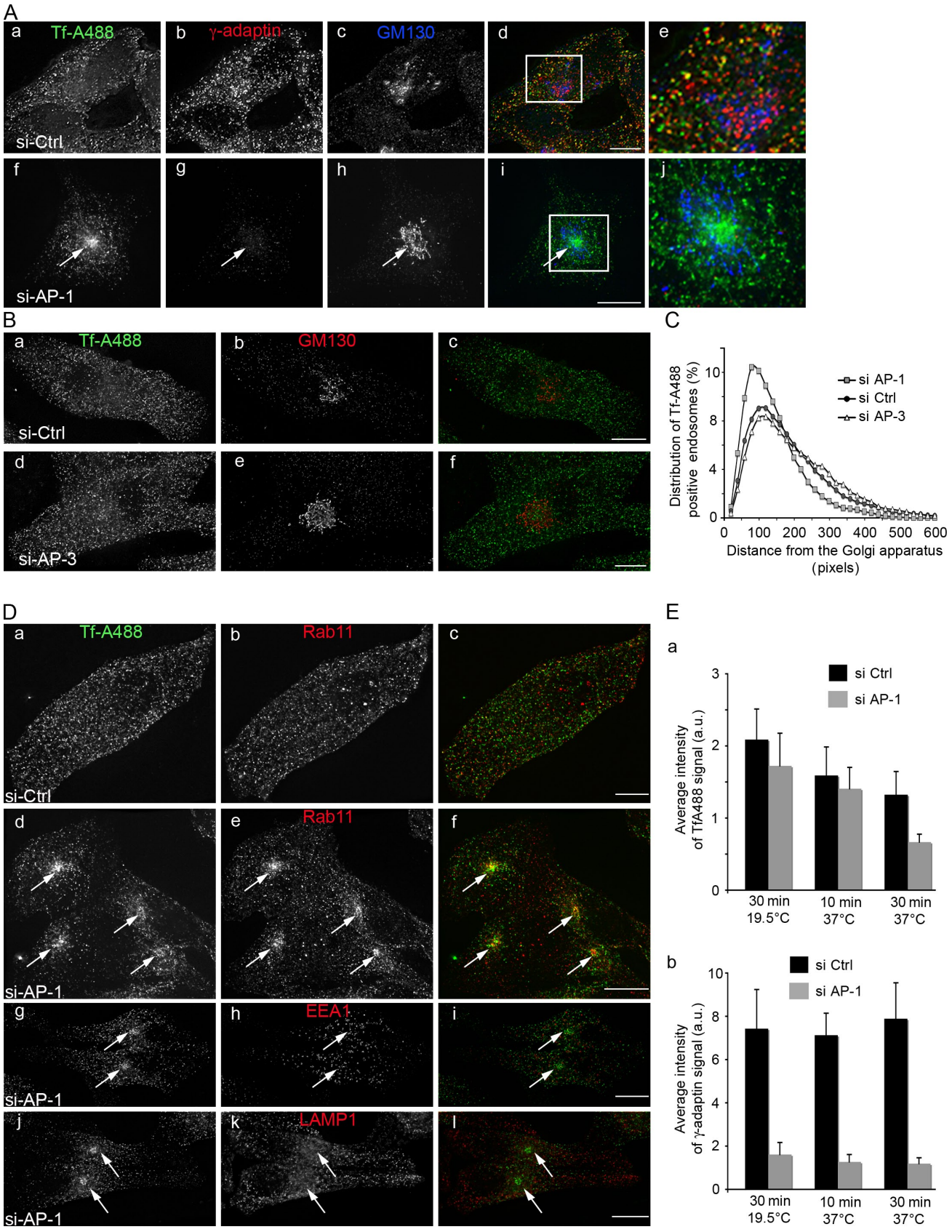

Figure 3. **AP-1 is required for the peripheral distribution of recycling endosomal domains.** (A) IFM analysis of MNT-1 cells treated with control (a–e) or μ1A/γ-adaptin (f–j) siRNAs that had internalized Tf-A488 for 45 min (a and f) and labeled for AP-1 (γ-adaptin; b and g) and the Golgi marker GM130 (c and h). Single labeling (columns 1–3), merged images (column 4), and magnified insets (of boxed areas; column 5) are shown. Note that Tf-A488–containing endosomes were clustered in the peri-Golgi area of AP-1–depleted cells (f–i, arrows). (B) MNT-1 cells treated with control (a–c) or β3A (d–f) siRNAs

RNA inhibition. Cells were treated with siRNAs to AP-1 subunits as in Fig. 1 B (Fig. 3, A and D) or to the β3A subunit of AP-3 as a control (Fig. 3 B). Remarkably, although in control cells recycling endosomal domains were evenly distributed, in cells treated with siRNA to μ1A or μ1A and γ-adaptin, a large fraction of them clustered near the Golgi (Fig. 3 A, compare a with f). This distribution, also apparent upon labeling for Rab11 (Fig. 3 D, compare b with e), resembled the pericentriolar accumulation of recycling endosomes in other cell types (Hopkins et al., 1994). Clustering was observed only upon depletion of AP-1 and not of the related AP-3 complex (Fig. 3 B) and was quantified as a substantial shift in the distribution of distances between the Tf-A488–labeled structures and the center of the Golgi (labeled for GM130; Fig. 3 C). Clustering was specific for subdomains of early recycling endosomes because the distribution of sorting endosomes and lysosomes, labeled by EEA1 and LAMP-1, respectively, was unchanged (Fig. 3 D, g–l). AP-1 depletion did not affect Tf internalization (measured as accumulation of Tf-A488 after 10 min of uptake at 37°C or after 30 min when inhibiting recycling at 19.5°C; Fig. 3 E) but did result in slightly more rapid Tf recycling (measured as loss of Tf-A488 fluorescence after 30 min of chase; Fig. 3 E, a), corroborating evidence that pericentriolar recycling endosomes facilitate efficient Tf recycling (Maxfield and McGraw, 2004). Collectively, these results indicate that AP-1 is required for the peripheral distribution of a cohort of recycling endosomal domains in melanocytic cells.

KIF13A cooperates with AP-1 for endosome polarization and melanosomal protein sorting

The loss of peripheral localization of endosomes upon AP-1 depletion might reflect a role for this adaptor at a step required for endosome motility toward melanosomes. AP-1 can physically associate with KIF13A (kinesin superfamily protein 13A), a plus end–directed microtubule motor of the kinesin family (Nakagawa et al., 2000). KIF13A, via interaction with AP-1, was proposed to mediate TGN to plasma membrane movement of vesicles containing the mannose 6-phosphate receptor (Nakagawa et al., 2000) and thus is a good candidate to mediate AP-1–dependent peripheralization of recycling endosomal domains in melanocytes. By IFM, KIF13A labeling in MNT-1 cells partially overlaps with peri-Golgi and peripheral AP-1 puncta (Fig. 4 A, a-d, arrows) and with Tf-loaded endosomes (Fig. 4 A, e–h, arrows), suggesting that a cohort of KIF13A functions with AP-1 within the endosomal system. By Western blot analysis, treatment with KIF13A-specific siRNA extinguishes a band corresponding to its predicted molecular weight (Fig. 4 B). As in other cell types (Nakagawa et al., 2000), the monomeric form of KIF13A is detected in anti–AP-1 immunoprecipitates from MNT-1 cell lysates (Fig. 4 C), and reciprocally, γ-adaptin is coimmunoprecipitated with anti-KIF13A (Fig. S3 C, bottom). This interaction is specific because preincubation of the lysate with a blocking peptide corresponding to the epitope recognized by the KIF13A antibody abolishes both KIF13A and γ-adaptin enrichment in immunoprecipitates (Fig. S3 C).

To test whether KIF13A functions in AP-1–dependent endosome positioning, we inactivated KIF13A using three different siRNAs that decreased steady-state KIF13A levels by 78, 82, and 53 ± 10% (Fig. 4 B and Fig. S3 B). As for AP-1 (Fig. 3 A), depletion of KIF13A results in the pericentriolar accumulation of a pool of recycling endosomal domains labeled by both Tf-A488 internalized for 30 min and Rab11 (Fig. 4 E, arrows). Quantification of the clustering of Tf-containing endosomes near the Golgi region showed that depletion of either KIF13A or AP-1 resulted in a nearly twofold increase in "compaction" relative to cells treated with control or AP-3 siRNA (Fig. 4 D). AP-1 was also redistributed upon KIF13A depletion (Fig. 4 F), resulting in a 60% increase in labeling near the TGN (Fig. 4 G). In contrast, as observed for AP-1 (Fig. S1, A, C, and E), KIF13A depletion did not affect the distribution of EEA1, LAMP-1, and Pmel17 (Fig. S3, d–l). To confirm the specificity of the phenotype, cells were analyzed 2 d after siRNA microinjection. Tf- and Rab11-containing recycling endosomes were clustered in 50% of cells microinjected with AP-1 or KIF13A siRNAs but not with control siRNA (Fig. S4 B). Finally, clustering of Tf- and Rab11-containing recycling endosomes was also observed upon expression of a dominant-negative form of KIF13A fused to GFP (Fig. S4 A, arrows). Together, these data show that KIF13A is required for the peripheral distribution of AP-1–positive recycling endosomal subdomains in melanocytes and suggest that AP-1 and KIF13A cooperate to target recycling endosomes toward the cell periphery.

If the KIF13A-dependent distribution of recycling endosomal domains is required for efficient transfer of selected cargoes from endosomes to melanosomes, KIF13A depletion should disrupt cargo delivery and consequent melanosome maturation. Consistent with this prediction, MNT-1 cells treated with KIF13A-specific siRNA have dramatically reduced numbers of mature melanosomes, as evaluated by conventional EM (Fig. 5 A), and a 40% reduction in melanin content (Fig. 5 D) relative to controls (Fig. 1, A [b] and G). Concomitantly, KIF13A-depleted cells accumulate vacuolar compartments similar to those observed in AP-1–depleted cells (Fig. 5 A, arrows) that accumulate Tyrp1 (Fig. 5 B, b, arrows) and that are dispersed throughout the cytoplasm (Fig. S3 A, n). In these cells, Tyrp1 is

that had internalized Tf-A488 for 45 min (a and d) were labeled for GM130 (b and e). Single labeling (columns 1 and 2) and merged images (column 3) are shown. (C) Quantitative evaluation of the distribution of Tf-positive endosomes in cells transfected with control, μ1A, or β3A siRNAs. Results are presented as a histogram of the mean distance (from >30 cells each) of Tf-loaded endosomes from the center of the Golgi apparatus labeled by GM130. (D) MNT-1 cells were treated with control (a–c) or μ1A-specific siRNAs (d–l), incubated with 10 μg/ml Tf-A488 for 45 min, fixed, labeled with antibodies to Rab11 (b and e), EEA1 (h), or LAMP-1 (k), and analyzed by IFM. In AP-1–inactivated cells as compared with control cells (a–c), note the peri-Golgi clustering of endosomes labeled with Tf-A488 and Rab11 (d–f, arrows) but not with EEA1 (g–i, arrows) or LAMP-1 (j–l, arrows). (E) Quantification of Tf accumulation in cells treated with control or μ1A/γ-adaptin siRNAs. Mean intensity of total Tf-A488 fluorescence (a) and γ-adaptin labeling (b) was measured and presented as mean ± SD. Bars, 10 μm.

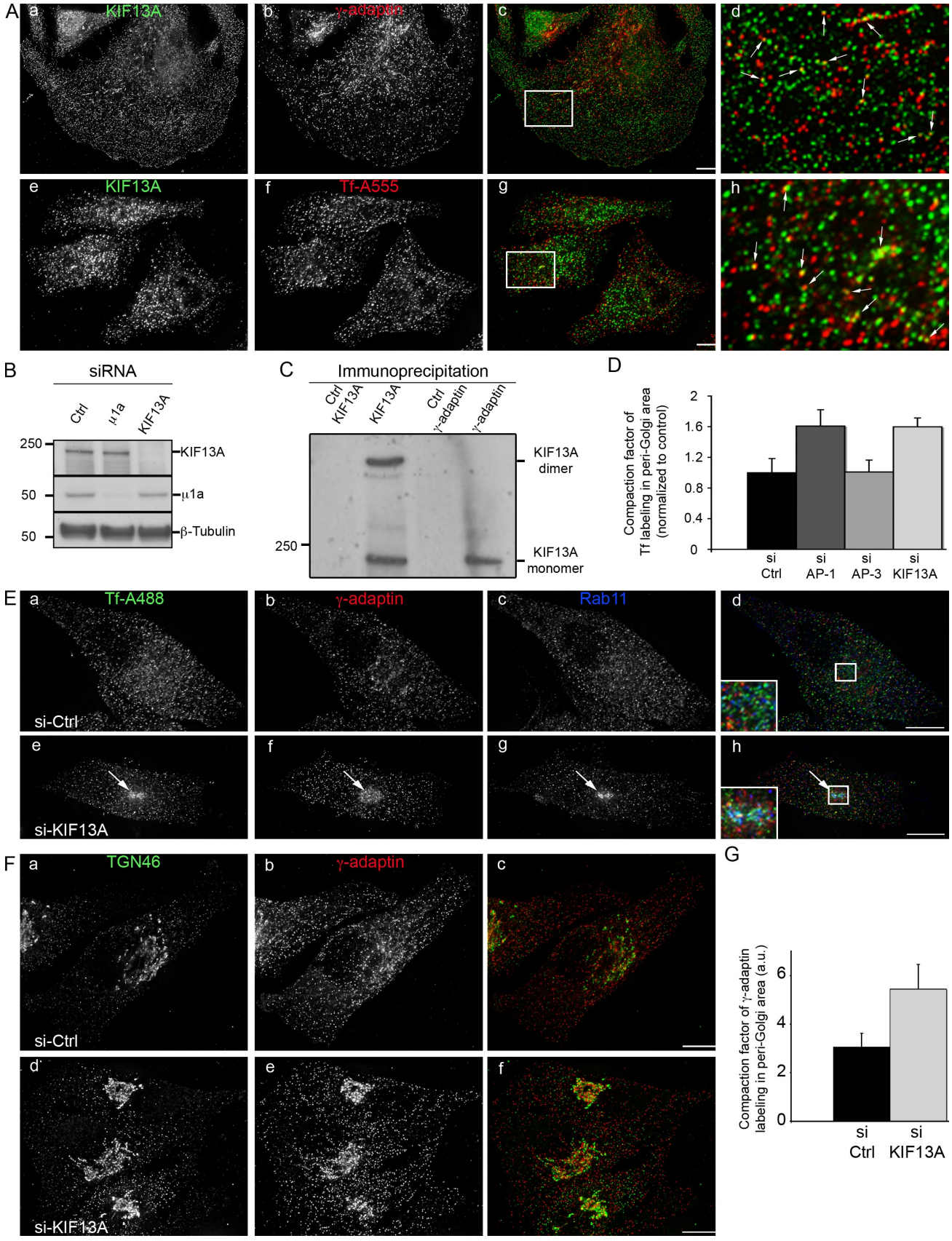

Figure 4. **AP-1 and KIF13A function together on the peripheral localization of recycling endosomes.** (A) MNT-1 cells were fixed in cold methanol, and endogenous KIF13A localization (a and d) was assessed relative to AP-1 (b) or Tf internalized for 45 min (f). Single labeling is shown in columns 1 and 2, merged images in column 3, and magnified insets (of boxed areas) in column 4. KIF13A-labeled tubular and punctate structures partially overlap with γ-adaptin (d, arrows) and internalized Tf (h, arrows). (B) Western blot analysis of lysates of cells treated with control (Ctrl), AP-1 (μ1a), or KIF13A siRNAs

nearly completely depleted from melanosomes and melanosome-associated tubulovesicular profiles (Fig. 5 C, right). Although more AP-1–coated vesicles accumulate near the TGN in KIF13A-depleted cells (Fig. 5 B, a, arrowheads) than in control cells (Fig. 5 C, left) as observed by IFM (Fig. 4, E and F), many of the peripheral vesicles are adjacent to the Tyrp1-containing vacuolar endosomes (Fig. 5, B [b, arrowheads] and C [left]), as expected for an interaction of AP-1 with the Tyrp1 sorting signal (Theos et al., 2005). Indeed, cross-linking experiments in control MNT-1 cells reveal a tripartite interaction between the motor, adaptor, and cargo; anti-Tyrp1 immunoprecipitates from lysates of cross-linked cells contained both γ-adaptin and KIF13A (Fig. 5 E). These data show that melanosomal cargoes interact with AP-1 and/or KIF13A and are trapped within endosomes in the absence of either KIF13A or AP-1. Thus, they indicate that the AP-1– and KIF13A-dependent formation of recycling endosomal tubules is required to deliver resident proteins to melanosomes and therefore to generate mature LROs in melanocytes. Moreover, they suggest that AP-1 has a dual function in both cargo sorting and tubule formation/positioning.

Endosomal tubules contact melanosomes and become continuous with the melanosomal membrane

Having shown that peripheral recycling endosomal domains are conduits for melanosomal cargoes, we next sought to define the physical nature of these domains; are they donor membranes from which vesicles emerge that then fuse with nearby melanosomes, or do they represent tubular structures that directly fuse with maturing melanosomes? To distinguish these possibilities, we used two approaches. First, we used live cell imaging to dissect the interactions between these domains and melanosomes in real time. MNT-1 cells were incubated with Tf-A488 for 30 min, and the fluorescent signal and bright field images (to visualize pigmented melanosomes) were acquired over 5 min by time-lapse confocal microscopy (Fig. 6 and Video 1). To better appreciate individual endosomes and melanosomes, the images were rendered binary (Angénieux et al., 2005). Many of the peripheral Tf-filled endosomal structures show a tubular morphology (Fig. 6 A), and many of the tubules extend toward and remain near (within 650 nm) melanosomes for prolonged times (e.g., Video 1, at 3 min 18 s; and Fig. 6, A [b] and B [arrows]). Importantly, individual tubules do not statically associate with melanosomes but rather form a network of tubular structures that extend and retract from Tf-containing puncta to neighboring melanosomes (Fig. 6 B, arrows; and Video 1). Nevertheless, Tf-A488 does not consistently overlap with melanosomes, even for a short period of time. This suggests that Tf-A488 is not appreciably delivered to melanosomes, corroborating IEM data (Fig. 2 C). These observations indicate that tubular endosomal domains dynamically contact melanosomes, which is consistent with a potential role in transient delivery of cell type–specific cargoes to maturing LROs.

To assess whether there is a spatial coincidence between Tf-A488 endosomes and melanosomes, the time-lapse images were subjected to quantitative analysis of the codistribution of endosomes and melanosomes. In the segmented images (Fig. 6 B), allowing tracking of each melanosome individually, the intensity of the Tf-A488 signal per pixel was measured within a radius of 645 nm (5 pixels) of each melanosome throughout the acquisition. The frequency of detection of the binned fluorescent signal within the entire cell (Fig. 6 C, black), representing proximity of endosomes to all melanosomes, was compared with the frequency within a limited region (Fig. 6 A, b) that is enriched in endosomes and melanosomes (Fig. 6 C, red). The overall distribution of Tf-A488 fluorescence intensity throughout the cell is broad. Although some melanosomes tracked over the time course have few closely apposed Tf-A488 endosomes (Fig. 6 C, left of the black diagram), others show a high frequency of contacts (Fig. 6 C, right of the black diagram). The estimated time of contact between endosomes and individual melanosomes in consecutive frames of the time-lapse image (Fig. 6 D, red) indicates that once an endosome is close to a melanosome, their contact will last for a defined period of time (∼10 frames/30 s) independently of their location in the cell and their respective densities.

To better appreciate these contacts, we analyzed the endosomal–melanosomal network in MNT-1 cells by EM in cells that were preserved by high pressure freezing (HPF) and freeze substitution. In thin sections, melanosomes are typically surrounded by smooth, tubular elements (Fig. 7, a, arrows; and Fig. S5 A, a, arrows) that are distinct from rough ER (Fig. 7, a). To define the interface between the tubular elements and melanosomes, we used double-tilt 3D electron tomography on 350–400-nm-thick sections (Hurbain et al., 2008). Double-tilt series were recorded in regions of MNT-1 cell cytoplasm enriched in late-stage melanosomes and processed for tomographic reconstruction. Merged tilt series and tomographic slices (with or without manual contours) of a single representative melanosome are shown in Fig. 7 (b–g) and Videos 2–4. Analysis of individual slices (Fig. 7, b–g) and the 3D model of this organelle (Fig. 7, h; and Video 5) and others like it (Fig. S5 A) reveals that the membrane of some of the tubular elements apposed to melanosomes is continuous with the limiting

using anti-KIF13A or anti-μ1A antibodies or anti–β-tubulin as a loading control. (C)Anti-KIF13A or γ-adaptin immunoprecipitates from MNT-1 cell lysates were fractionated by SDS-PAGE and immunoblotted using KIF13A antibodies. Anti-KIF13A immunoprecipitates contain two bands corresponding to the monomeric and dimeric forms. Anti–γ-adaptin immunoprecipitates contain only the monomeric form. (D) MNT-1 cells were treated with control, μ1A, β3A, or KIF13A siRNAs and analyzed by IFM after internalization of Tf-A488. The intensity of fluorescence in the peri-Golgi area was evaluated as a compaction factor. Data were normalized to the control and presented as mean ± SD. (E) After internalization of Tf-A488 (a and e), control (a–d) and KIF13A (e–h) siRNA–treated cells were fixed and double labeled for γ-adaptin (b and f) and Rab11 (c and g). Depletion of KIF13A results in peri-Golgi clustering of Tf-A488– and Rab11-positive endosomes (e, g, and h, arrows). Merged images and magnified insets (of boxed areas) are shown in column 4. (F) IFM analysis of control (a–c) and KIF13A (d–f) siRNA–treated cells that were double labeled for TGN46 (a and d) and γ-adaptin (b and e). (G) The distribution of γ-adaptin labeling in the vicinity of the Golgi was measured in cells treated with control or KIF13A siRNAs. (B and C) Molecular masses are given in kilodaltons. Bars, 10 μm.

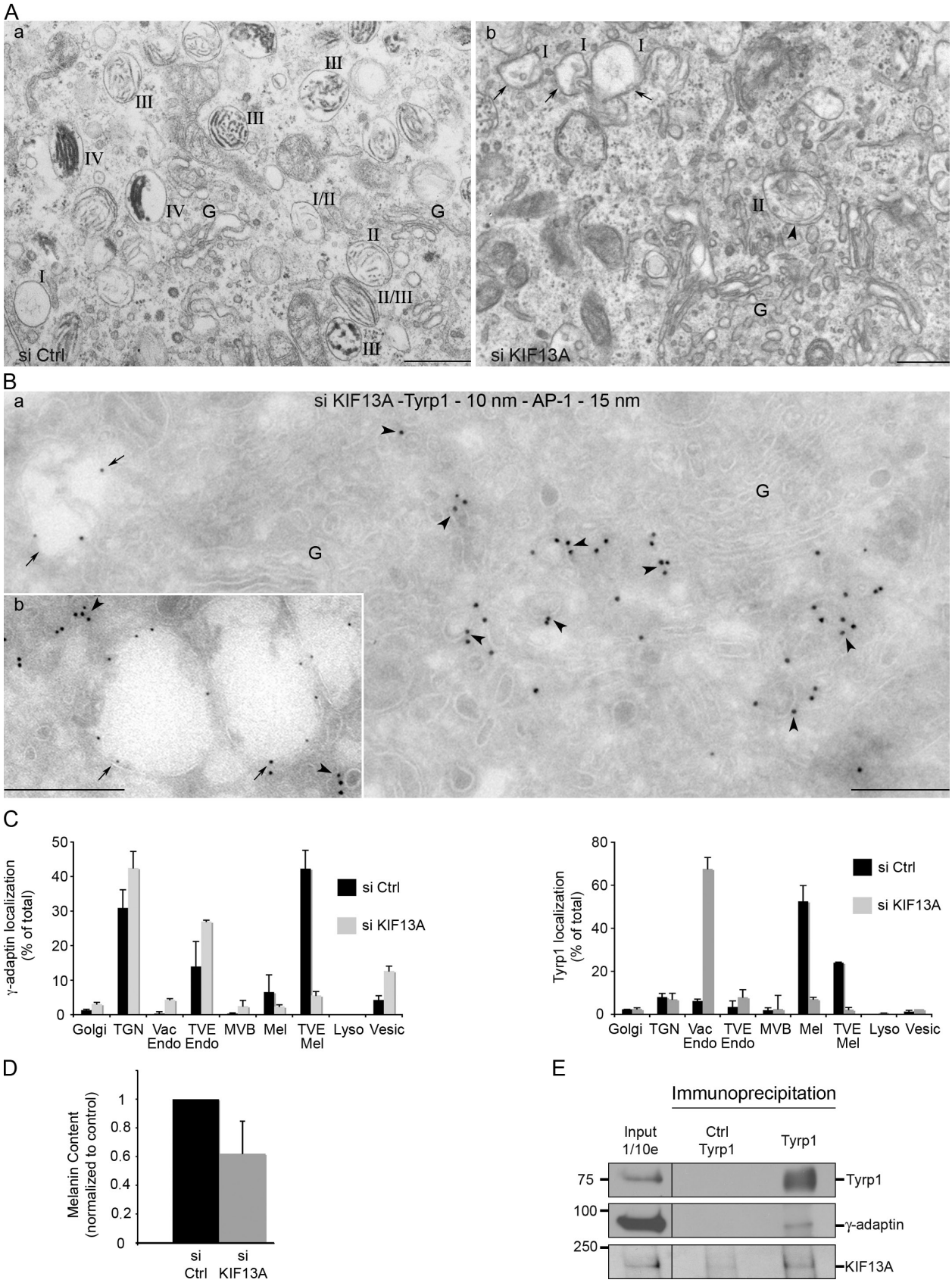

Figure 5. **Depletion of KIF13A inhibits melanogenesis and results in Tyrp1 accumulation in endosomal vacuoles.** (A) Cells treated with control (a) or KIF13A (b) siRNAs were analyzed by conventional EM. KIF13A-depleted cells accumulate vacuoles with internal membrane vesicles (arrows). Stage II premelanosomes are not affected (arrowhead). (B) KIF13A-depleted cells were analyzed by IEM. Ultrathin cryosections were labeled for AP-1 (PAG15) and Tyrp1 (PAG10). Tyrp1 localizes to the limiting membrane of endosomal vacuoles (a and b, arrows). An enrichment of AP-1–positive vesicles are observed

melanosomal membrane (Fig. 7, c–h, arrows; note the green color from the red lumenal leaflet of the melanosome membrane in g and h). To test whether these tubules represented the recycling endosomal domains shown in aforementioned figures, MNT-1 cells were analyzed by 3D tomography after they had internalized Tf-HRP for 45 min to fill recycling endosomal domains. Cells were chemically fixed (because of experimental constraints), and HRP activity was detected histochemically. As shown in Fig. S5 B (a and b), the tubular elements (Fig. S5 B, arrows) apposed to melanosomes are filled with Tf-HRP, showing that they correspond to early endosomes (note that the contrast required to detect the electron-dense HRP reaction product precludes consistent detection of membranes in these images). In several cell profiles, the Tf-HRP–positive/melanosome-proximal tubules emanate from vacuolar endosomal domains (Fig. S5, B [a, arrows] and C [arrows]), identifying them as recycling endosomes. Thick sections of the same cells were processed for tomographic reconstruction. Tomographic slices before and after manual contouring (Fig. S5 B, c and d; and Videos 6 and 7) and the deduced 3D models (Fig. S5, B [e and f] and C [e and f]; and Video 8) highlight the continuities between the melanosome and the Tf-HRP–filled tubules that emanate from the vacuolar endosome (Fig. S5 C, d and e, arrows; and Videos 9 and 10). These observations show that the limiting membranes of melanosomes establish physical connections by fusing with endosomal tubules.

Discussion

The endosomal recycling system subserves ubiquitous functions such as constitutive membrane recycling to the plasma membrane, retrograde membrane transport to the Golgi, cytokinesis, and cell–cell adhesion (van Ijzendoorn, 2006; Gould and Lippincott-Schwartz, 2009). Subcompartmentalization of this system is further specialized for essential processes such as cell polarity, phagocytosis, cell fate decisions, organelle generation, and regulated secretion (Bajno et al., 2000; Dugani and Klip, 2005; Perret et al., 2005; Manderson et al., 2007; Uzan-Gafsou et al., 2007; Gould and Lippincott-Schwartz, 2009). These properties imply that different molecular machineries associate with recycling endosomal membranes to generate specialized subdomains. In this study, we show that the adaptor protein complex, AP-1, and an interacting microtubule motor, KIF13A, cooperate to generate recycling endosomal domains that are specified for communication with melanosomes, the melanocyte LRO. Importantly, these effectors cooperate both in cargo sorting and in positioning endosomes toward the cell periphery near melanosomes, permitting the formation of interorganellar tubular connections.

AP-1 in melanosomal cargo recognition has been previously implicated (Theos et al., 2005; Chapuy et al., 2008), but where and how AP-1 functions in melanosome cargo delivery remained unclear. We show that AP-1A is enriched on buds emerging from Tf-containing endosomal tubules that partially overlap with Rab11 and that are adjacent to melanosomes. Thus, AP-1A functions predominantly on recycling endosomes in melanocytic cells, which is consistent with its role as an endosomal adaptor in other cell types (Le Borgne and Hoflack, 1997; Meyer et al., 2000). Moreover, we show that AP-1 is not only required to sort the melanosomal cargo protein Tyrp1 from endosomal domains toward melanosomes, but we also show that it is required for the positioning of these domains. Thus, AP-1 performs a dual function in melanocytic cells, sorting and positioning, both of which are required for efficient cargo delivery to maturing organelles.

The sorting function of AP-1 on endosomes is likely mediated by interactions with the cytoplasmic domains of Tyrp1 and other melanosomal proteins (Theos et al., 2005; Sitaram et al., 2009). In the absence of functional AP-1, Tyrp1 becomes trapped in endosomal vacuoles, indicating that the interactions with AP-1 are required to draw Tyrp1 and perhaps other associated cargoes from the vacuoles into tubulovesicular intermediates bound for melanosomes. In contrast to melanosomal cargoes, the trafficking of bonafide recycling endosomal cargoes (e.g., the Tf receptor) appears to be AP-1 independent because AP-1 depletion does not grossly affect the rate of Tf internalization and modestly increases, rather than decreases, the rate of Tf recycling.

Through its effect on organelle positioning, AP-1 adds a novel function to recycling endosome subdomains in addition to their ubiquitous function in recycling. Indeed, the increased recycling of Tf in AP-1–depleted melanocytes likely reflects Tf recovery in pericentriolar recycling domains from a cohort of endosomes that are engaged with melanosomes in which Tf is entrapped. Despite this entrapment, protein sorting between the tubules and melanosomes is regulated; although Tyrp1 is present in both the tubules and melanosomes, Tf in the tubules is actively excluded from melanosomes as indicated by the absence of internalized Tf conjugates in melanosomes by EM and by the absence of Tf delivery to melanosomes by video microscopy. This suggests that receptor-bound Tf is either rapidly removed from melanosomes after fusion or efficiently excluded from entry. Extensive further analyses will be required to distinguish these two possibilities.

Interestingly, AP-1 localizes in melanocytes (Raposo et al., 2001; this study) and other cell types (Waguri et al., 2003; Håberg et al., 2008) not only to buds, implying a role in vesicle formation, but also to tubules, supporting a role in tubule

in the vicinity of the Golgi apparatus (a, arrowheads) and close to the vacuoles (b, arrowheads). (C) Quantification of immunogold labeling for AP-1 (left) or Tyrp1 (right) on ultrathin cryosections. Localization of an equivalent number of gold particles in each sample was assessed relative to the indicated cell compartments. (D) Evaluation of melanin content of cells treated with control or KIF13A siRNAs. (E) MNT-1 cells were cross-linked with DSP, lysed, and immunoprecipitated with Tyrp1 antibody. Immunoprecipitates were reduced in sample buffer to cleave the cross-linker, fractionated by SDS-PAGE, and immunoblotted using antibodies to Tyrp1, γ-adaptin, or KIF13A. Black lines indicate that intervening lanes have been spliced out. Molecular masses are given in kilodaltons. G, Golgi apparatus; I–IV, stages I–IV; Vac Endo, vacuolar endosome; TVE Endo, tubulovesicular endosomes associated to endosomes; MVB, multivesicular body; Mel, melanosome; TVE Mel, tubulovesicular endosomes associated to melanosomes; Lyso, lysosome; Vesic, vesicle. Data are presented as mean ± SD. Bars, 200 nm.

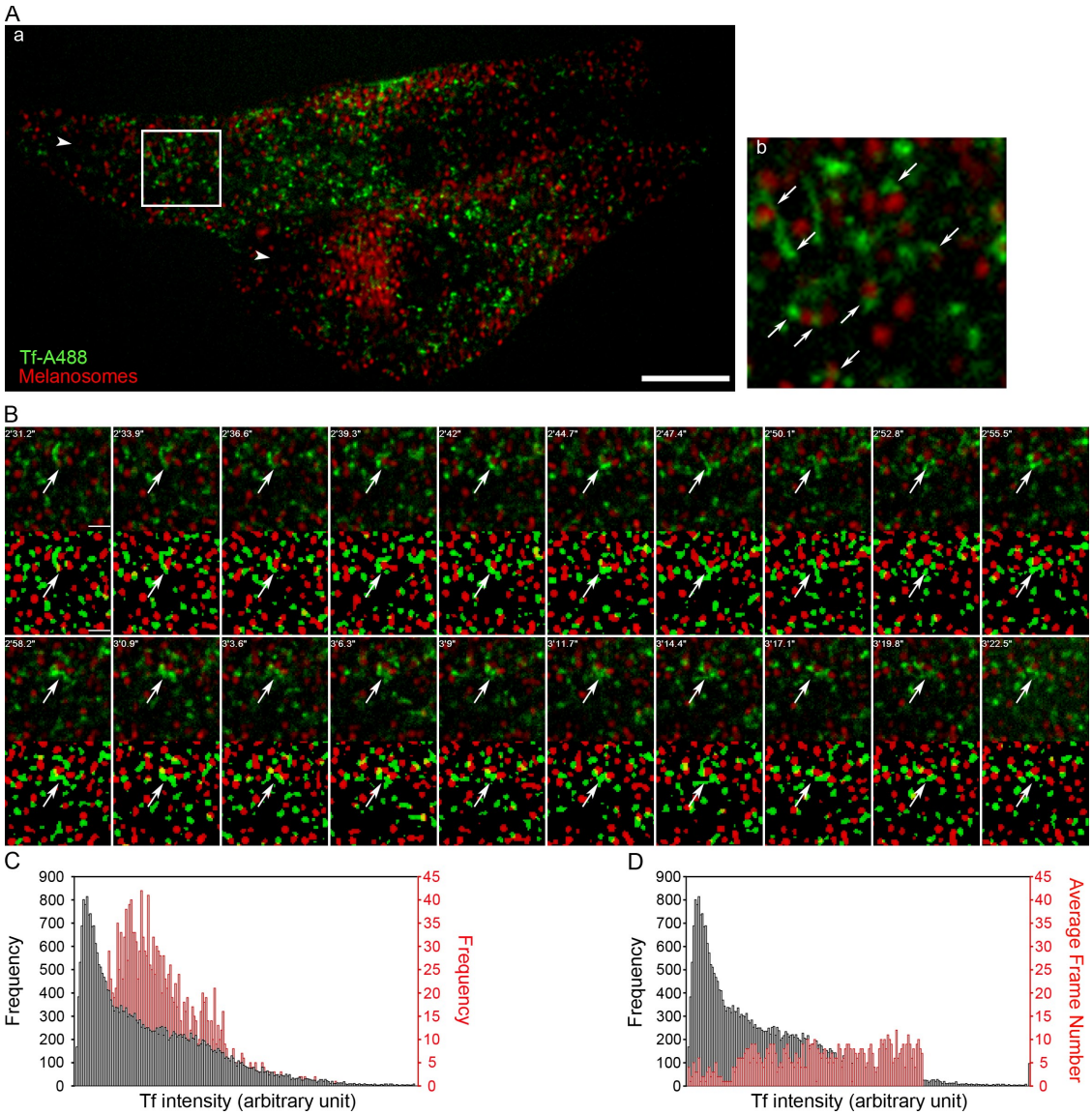

Figure 6. **Endosomal tubules dynamically contact melanosomes.** (A) Spinning-disc confocal microscopy was used to capture concomitant movements of Tf-positive endosomes (green) and melanosomes (red). (a) View of an entire cell at 30 min after Tf uptake and a magnified view of the boxed area (b) are shown. Fluorescently labeled endosomes are distributed throughout the cell and are frequently observed in close contact with melanosomes as shown in the inset (b, arrows). Note that in regions of the cell with fewer melanosomes (e.g., at the periphery of the cell), Tf-positive endosomes also appear to contact melanosomes (a, arrowheads). (B) Consecutive time-lapse images and corresponding binary-rendered images of the boxed region illustrated in A during 50 s are presented as a gallery. Note that melanosomes are found in close contact with endosomes (arrows). (C) The intensity of the Tf-A488 signal within 5 pixels (645 nm) of melanosomes was measured during the length of the time-lapse acquisition. Graphs represent the frequency of distribution of binned Tf-A488 intensities in the vicinity of all tracked melanosomes in the cell (black graph) and all melanosomes within the boxed region in A (red graph). Note the coincidence between both melanosome and endosome densities. (D) The intensity of the Tf-A488 signal was measured as in C, and the averaged time (mean frame number) of contact between individual, tracked melanosomes with individual Tf-A488–binned objects (red graph) was evaluated. Note that the time of contact between melanosomes and endosomes is stable regardless of the density of melanosomes (Video 1). Bars: (A) 10 µm; (B) 2 µm.

formation. Membrane tubulation is largely dependent on cytoskeletal elements, particularly microtubules (Roux et al., 2002), and thus, it is likely that AP-1 favors endosome tubulation via direct or indirect interactions with microtubule-associated proteins (Orzech et al., 2001) and motors such as KIF13A (Nakagawa et al., 2000) or KIF5B, as reported recently (Schmidt et al., 2009). Although KIF5B and KIF13A seem to share some similar properties, KIF5B localizes to the pericentriolar region and seems to favor AP-1–dependent transport of TGN-derived endosomal vesicles (Schmidt et al., 2009), whereas our data indicate that KIF13A tonically positions recycling endosomes toward the periphery and likely pulls tubules from vacuolar domains toward melanosomes. This conclusion is supported by (a) coprecipitation of AP-1 and KIF13A from MNT-1 cell lysates, (b) partial overlap of the endogenous KIF13A with peripherally distributed AP-1 and Tf, and (c) pericentriolar clustering of AP-1 and Tf/Rab11 recycling endosome domains in KIF13A-negative cells. The hypothesis that these features regulate melanosome cargo delivery is supported by the detection of both AP-1 and KIF13A in anti-Tyrp1 immunoprecipitates and by the

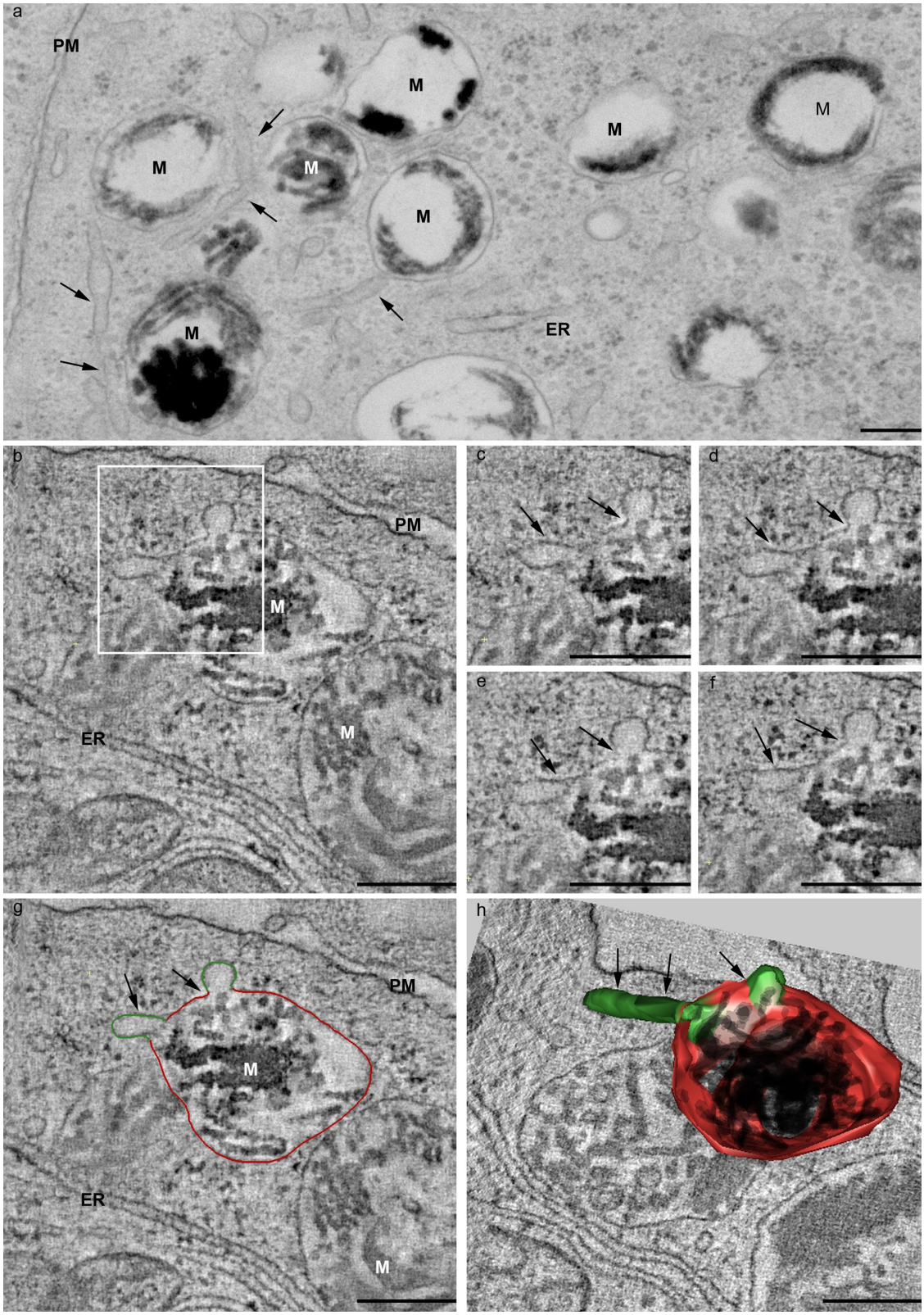

Figure 7. **Endosomal tubules are continuous with the melanosome limiting membrane.** (a) Low magnification EM analysis of thin sections of MNT-1 cells fixed by HPF. Several smooth tubules are close to and surround melanosomes (arrows). Note the distinction of these smooth tubules from the rough ribosome-studded ER. (b–f) Successive slices through the tomographic volume highlight continuities between the vesicular/tubular membranes and the melanosomal membrane (arrows). The ER, studded with ribosomes, is close to the melanosome but does not show continuities. Insets show magnified views of the boxed area. (g and h) Membranes in consecutive tomogram slices are manually contoured; one slice is shown in g, and the deduced 3D model is shown in h. Tubular membranes (green) that are continuous with the melanosome limiting membrane (red) are indicated by arrows. See Video 2 for tilt images, Video 3 for tomographic reconstruction, Video 4 for manual contouring, and Video 5 for a 3D model. M, melanosome; PM, plasma membrane. Bars, 200 nm.

inhibition of melanogenesis and impairment of Tyrp1 trafficking from vacuolar endosomes in cells depleted of either AP-1 or KIF13A. Based on these data, we propose the following speculative model (Fig. 8): (1) via interaction with cytoplasmic targeting signals, AP-1 recruits melanosomal cargoes (e.g., Tyrp1) into endosomal domains in a clathrin-dependent manner; (2) after clathrin uncoating (Nakagawa et al., 2000), AP-1 engages KIF13A to position endosomes along microtubules toward the cell periphery where contacts with melanosomes are favored; endosome positioning is likely followed by clathrin reassociation with AP-1 because the AP-1–coated buds close to melanosomes are clathrin coated; and (3) this mechanism would facilitate transfer of enzymes and transporters required for melanogenesis and could be similarly exploited by other specialized cell types that require "polarized" endosomal delivery of membrane cargoes. The requirement for AP-1 in LRO biogenesis in melanocytes parallels a similar requirement for AP-1 and its binding partners at an early step in Weibel–Palade body biogenesis in endothelial cells (Lui-Roberts et al., 2005).

An essential role for early endosomes as intermediates for transport of melanosomal enzymes to melanosomes was previously supported by analysis of melanocytes from AP-3– and BLOC-1–deficient HPS patients and mouse models (Huizing et al., 2001; Theos et al., 2005; Setty et al., 2007). The genes encoding AP-1 subunits and KIF13A are not among the characterized HPS mutants (Wei, 2006), likely because AP-1 (Meyer et al., 2000) and perhaps KIF13A are essential in mammals. In this study, we show that the coordinated action of AP-1 and KIF13A complements HPS-encoded protein complexes to maintain functional endosome–melanosome cross talks and permit LRO maturation. It is noteworthy that BLOC-1 subunits, like AP-1, are detected on the melanosome-proximal endosomal tubules (Di Pietro et al., 2006). Moreover, AP-1– and KIF13A-depleted cells share features with BLOC-1–deficient HPS mouse melanocytes. Indeed, BLOC-1–deficient melanocytes are severely hypopigmented and accumulate endosomal vacuoles in which Tyrp1 is entrapped (Setty et al., 2007, 2008). This phenotype is distinct from that observed in AP-3–deficient melanocytes in which Tyrp1 trafficking through endosomes is not disrupted (Huizing et al., 2001; Theos et al., 2005). Although BLOC-1 interacts biochemically with AP-3 (Di Pietro et al., 2006; Salazar et al., 2006) and there is yet no evidence for interactions between BLOC-1 and AP-1, it is nevertheless tempting to speculate that BLOC-1 perhaps cooperates indirectly with AP-1 in cargo delivery via specialized endosomal tubules.

The endosomal domains from which AP-1 and KIF13A function in melanocytes are derived from the endosomal recycling system based on the unique positioning of Rab11 and of internalized Tf after long chase periods. The hypothesis that these peripherally distributed endosomal domains undergo transient fusion events with melanosomes is supported by both live cell imaging and static electron tomography analyses. The tubules are not induced by Tf uptake and appear to correspond to a constitutive pool of endosomes that can establish close cross talks with melanosomes because they are seen by electron tomography in the absence of Tf uptake. The presence in these tubules of BLOC-1 (Di Pietro et al., 2006) and Tyrp1, but not the premelanosomal protein Pmel17, strongly supports their function as conduits for cargo into and/or out of maturing melanosomes. Therefore, our study provides evidence for the transfer of cargoes between early endosomes and postendosomal organelles via direct tubular connections rather than vesicular transport as has been reported during kiss and run fusion of late endosomes and lysosomes (Bright et al., 2005). Interestingly, maturation of cytolytic granules, cytotoxic T cells LRO, also requires fusion events with endosomal compartments (Ménager et al., 2007). It is therefore possible that analogous mechanisms operate for the generation of multiple LROs.

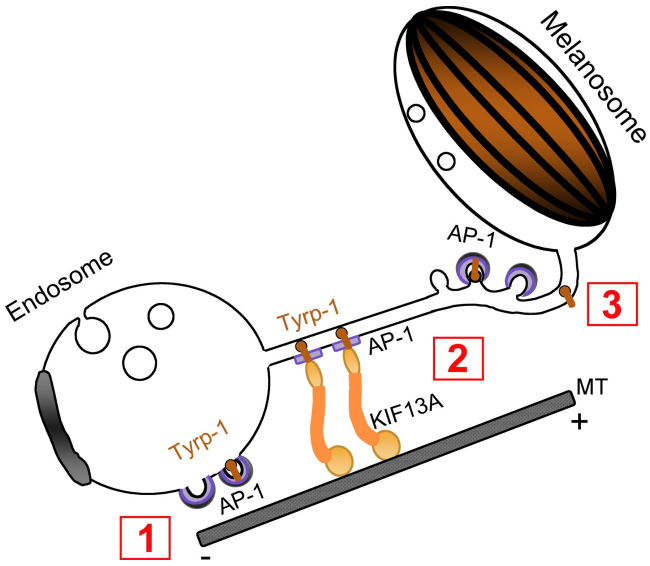

Figure 8. **Model for AP-1 and KIF13A function in Tyrp1 sorting and endosome positioning.** AP-1 is recruited to endosomes through its interaction with the sorting signal in the cytoplasmic domain of Tyrp1 (step 1). Further interaction of AP-1 with KIF13A (step 2) facilitates endosome tubulation and extension to the periphery of the cell along microtubules (MT). The endosomal tubules coated with AP-1 contact melanosomes with which they can fuse to deliver cargo (step 3).

In conclusion, we propose that interactions between an adaptor protein complex and a molecular motor link cargo sorting and endosome positioning to create specialized subdomains of the endosomal recycling system that can be used as gated conduits by which only cell type–specific cargoes are delivered to maturing LRO. How this gateway is maintained is not known but might be the target of mutation in genetic diseases such as HPS.

Materials and methods

Antibodies

Mouse monoclonal anti-Tyrp1 (ab3312), HMB-45 to Pmel17 (ab787), anti-EEA1 (ab15846), anti-CD9 (ab19761), and rabbit polyclonal anti–β-tubulin (ab6046) were obtained from Abcam. Mouse monoclonal H4A3 to human LAMP-1 was obtained from BD. Sheep anti–human TGN46 was obtained from AbD Serotec, mouse monoclonal anti–γ-adaptin (clone 100/3) was obtained from Sigma-Aldrich, anti-GM130 rabbit polyclonal antibody was obtained from EMD, and rabbit polyclonal to KIF13A was obtained from Bethyl Laboratories, Inc. (A301-077A). The rabbit polyclonal antibody to full-length recombinant Rab11A was described previously (Wilcke et al., 2000). Rabbit polyclonal antibodies to μ1a and EEA1 and the mouse mAb (SA4) to the AP-3 δ subunit were provided

by L. Traub (University of Pittsburgh, Pittsburgh, PA), M.J. Clague (University of Liverpool, Liverpool, England, UK), and A.A. Peden (University of Cambridge, Cambridge, England, UK), respectively. Tf-A488 and -A555 were obtained from Invitrogen, HRP-conjugated Tf was provided by G. LeDez and P. Chavrier (Institut Curie, Centre National de la Recherche Scientifique, Paris, France), and secondary goat anti–rabbit or –mouse antibodies conjugated to Alexa Fluor 488, 555, or 647 were obtained from Invitrogen. Protein A conjugated to 10- or 15-nm gold particles was obtained from the Cell Microscopy Center (Utrecht University Hospital, Utrecht, Netherlands).

Cell culture and siRNA depletion
MNT-1 cells were maintained in DME supplemented with 20% FBS (Invitrogen) as previously described (Raposo et al., 2001), and transfection with oligonucleotides proceeded as reported previously (Theos et al., 2006). 1×10^6 cells were seeded in a 10-cm dish at day 1 and transfected on day 3 with 40 pmol siRNA according to the manufacturer's instructions (Oligofectamine; Invitrogen). At day 4, 1×10^5 transfected cells were seeded in 6-well plates and were either transfected or not a second time at day 5. Cells were collected at day 5 or 7 and processed for melanin quantification assays (Wasmeier et al., 2006), IFM, EM, and Western blotting. The level of expression of each corresponding protein was assessed by Western blotting using specific antibodies and compared with β-tubulin expression as a loading control.

Oligonucleotides used in siRNA experiments
The sense strand for the indicated double-stranded siRNAs were synthesized with the following sequences or derived from the following references: siRNA control, 5′-AATTCTCCGAACGTGTCACGT-3′; siRNA μ1a #1, 5′-AAGGCATCAAGTATCGGAAGA-3′ (Hirst et al., 2003); siRNA μ1a #2, 5′-CCCGATCAGTGTCAAGTTCGA-3′ (QIAGEN); siRNA γ-adaptin, 5′-ACCGAATTAAGAAAGTGGT-3′; siRNA β3A, 5′-ATGGCTGATCTTGAAGGTTTA-3′ (Lui-Roberts et al., 2005); KIF13A siRNA, sc-43380 (Santa Cruz Biotechnology, Inc.); siRNA KIF13A #2, 5′-CTGGCGGGTAGCGAAAGAGTA-3′ (QIAGEN); and siRNA KIF13A #3, 5′-CCGCAACAACTTGGTAGGAAA-3′ (QIAGEN).

Microinjection of siRNAs
Microinjection of MNT-1 cells grown on 35-mm glass coverslips was performed using a manual microinjector (TransferMan NK2; Eppendorf). 5 μM of the corresponding siRNA was diluted in the microinjection buffer (5 mM phosphate sodium buffer, pH 7.2, and 100 mM KCl) supplemented with 1 μM Texas red–conjugated dextran (Invitrogen), which was used as a microinjection marker.

Plasmids
Full-length KIF13A cDNA (Thermo Fisher Scientific) was prepared from bacteria using the Plasmid Mini kit (QIAGEN), and the tail corresponding sequence (nucleotides 3,919–5,310, corresponding to the last 464 amino acids of KIF13A) was amplified by PCR. The sequence corresponding to the KIF13A tail domain was verified and cloned in mammalian expression vectors with the N-terminal GFP tag using a cloning system according to the manufacturer's instructions (Gateway; Invitrogen). pSPOII-GFP was provided by E. Bertrand (Institut de Génétique Moléculaire de Montpellier, Montpellier, France; Boulon et al., 2008).

Cross-linking and immunoprecipitations
MNT-1 cells at 80% of confluency were washed in cold PBS and lysed on ice in lysis buffer (50 mM Tris, 150 mM NaCl, 0.1% Triton X-100, 10 mM EDTA, pH 7.2, and protease inhibitor cocktail [Roche]). For cross-linking experiments, three dishes per condition were incubated with 1 mM DSP (dithiobis[succinimidyl propionate]; Thermo Fisher Scientific) in 1% DMSO or in 1% DMSO alone in cross-linking buffer (150 mM NaCl, 0.2 mM $CaCl_2$, 0.2 mM $MgCl_2$, and 10 mM Hepes, pH 7.3) for 30 min at 4°C, neutralized with three washes in 150 mM NaCl and 20 mM Tris, pH 7.3, and lysed on ice in lysis buffer. Then, lysate was first precleared using protein G agarose beads for 1 h at 4°C under rotation. Supernatants were collected and incubated with protein G agarose beads with 1 μg rabbit anti–human IgG or 1 μg mouse monoclonal IgG_{2b} anti-CD9 for 1 h at 4°C. To immunoprecipitate KIF13A, γ-adaptin, or Tyrp1, supernatants were incubated with beads coated earlier with 1 μg anti-KIF13A polyclonal antibodies, 1 μg mouse monoclonal IgG_{2b} anti–γ-adaptin, or 1 ml TA99 supernatant, respectively, for 2 h at 4°C under rotation. As controls, 1 μg rabbit anti–human IgG and 1 μg mouse monoclonal IgG_{2b} anti-CD9 were used to immunoprecipitate the lysate. After three washes in cold lysis buffer, immunoprecipitated proteins bound to the beads were incubated in sample buffer with reducing agent, boiled, and fractionated by SDS-PAGE using Nupage (3–8%) Tris-acetate gels (Invitrogen) for Western blotting detection of KIF13A and cross-linked proteins or Nupage (4–12%) Bis-Tris gels (Invitrogen) to reveal γ-adaptin. Material was transferred on nitrocellulose membrane (Millipore) to XCell II Blot Module (Invitrogen) and detected using KIF13A and γ-adaptin antibodies.

Tf uptake, immunofluorescence, and time-lapse fluorescence microscopy
MNT-1 cells were washed in FBS (GIBCO), then in PBS, and starved for 45 min in DME at 37°C in 5% CO_2. Cells were further incubated in DME supplemented with Tf-A488 or Tf-A555 at a final concentration of 10 μg/ml for 30 min at 37°C in 5% CO_2. Cells were washed in PBS at 37°C and fixed for 10 min at RT in 4% PFA except for KIF13A labeling, in which cells were fixed in cold methanol followed by incubation in PBS and 1 mg/ml BSA (blocking buffer) all along the procedure. Fixed cells were washed in PBS, quenched for 10 min in PBS and 50 mM glycine at RT, saturated in blocking buffer, and permeabilized in PBS, 0.05% saponin, and 1 mg/ml BSA (incubation buffer [IB]). Cells were incubated for 45 min with the primary antibody diluted in IB, washed three times in IB, and incubated with the corresponding secondary antibody for 30 min. Cells were washed twice in IB and once in blocking buffer. Finally, coverslips were mounted in DABCO medium and examined under a 3D deconvolution microscope (DM-RXA2; Leica) equipped with a piezo z drive (Physik Instrument) and a 100 × 1.4 NA Plan Apo objective lens for optical sectioning. 3D multicolor image stacks were acquired using MetaMorph software (MDS Analytical Technologies) through a cooled charge-coupled device (CCD) camera (Coolsnap HQ; Photometrics). All IFM images are deconvoluted and maximum intensity z projections (Figs. 1–4, S1, and S3; Sibarita, 2005). For time-lapse microscopy, MNT-1 cells grown on glass coverslips were transferred just before observation to custom-built aluminum microscope slide chambers (Ludin chamber; Life Imaging Services) filled with culture medium supplemented with10 μg/ml Tf-A488 and 10 mM Hepes. Time-lapse imaging was performed at 37°C (Life Imaging Services) using a spinning-disk microscope mounted on an inverted motorized microscope (TE2000-U; Nikon) through a 100 × 1.4 NA Plan Apo objective lens. The apparatus is composed of a spinning-disk head (CSU-22; Yokogawa), a laser lounge (with a 491-nm Cobalt for GFP observation; Roper Industries), a CCD camera (Coolsnap HQ2; Photometrics) for image acquisition, and MetaMorph software to control the setup. The acquisition parameters used were 200-ms exposure for A-488 channel and 30 ms for bright field.

Tf-endocytosis assay
Control and AP-1–inactivated MNT-1 cells were starved for 30 min and incubated for 30 min with 10 μg/ml Tf-A488 at 19.5°C to accumulate Tf in early endosomal compartments. Medium was removed and replaced with prewarmed complete medium, the temperature was shifted to 37°C, and Tf was chased for 10 and 30 min. Cells were fixed at each time point and immunolabeled with anti–γ-adaptin antibodies to identify inactivated cells. Images were acquired under a 3D deconvolution microscope and processed for deconvolution. The total Tf-A488 fluorescence and γ-adaptin labeling intensity were measured and averaged using MetaMorph software.

EM
For conventional EM, control and inactivated MNT-1 cells grown on coverslips were fixed with 2.5% glutaraldehyde in 0.1 M cacodylate buffer for 24 h and processed as described previously (Raposo et al., 2001). For ultrathin cryosectioning and immunogold labeling, cells were fixed with 2% PFA or with a mixture of 2% PFA and 0.2% glutaraldehyde in 0.1 M phosphate buffer, pH 7.4. Cells were processed for ultracryomicrotomy and single- or double-immunogold labeled using protein A conjugated to 10 nm gold (PAG10) or 15 nm gold (PAG15) as reported previously (Theos et al., 2005). Sections were observed under an electron microscope (Philips CM120; FEI Company), and digital acquisitions were made with a numeric camera (Keen View; Soft Imaging System).

Internalization of Tf-HRP
MNT-1 grown on glass coverslips for 2 d were starved for 45 min in DME and incubated with DME supplemented with 25 μg/ml Tf-HRP for 30 min. Cells were rapidly washed in DME at 4°C and fixed for 90 min with a mixture of 2% PFA/0.5% glutaraldehyde in 0.2 M phosphate buffer, pH 7.4. To reveal HRP, cells were washed three times for 5 min in 50 mM Tris-HCl, pH 6.85, and incubated with 1.5 mg/ml DAB for 30 min followed by a 1-h incubation with 1.5 mg/ml DAB supplemented with 0.5% H_2O_2. Cells were fixed with 2.5% glutaraldehyde in 0.1 M cacodylate buffer for

90 min, postfixed with 2% OsO_4, dehydrated in ethanol, and embedded in epon. Ultrathin (60–70 nm) or thick (300–400 nm) sections were observed at 80 or 200 kV for electron tomography (see following paragraph).

Electron tomography

MNT-1 cells were grown on carbonated sapphire discs at 70% confluency and were high pressure frozen with a high pressure freezer (EM PACT I; Leica), freeze substituted in a freeze substitution system (AFS; Leica), and embedded in epon 812 (TAAB Laboratories Equipment Ltd.) as described previously (Hurbain et al., 2008). Tomographic acquisitions made on thick 350-nm sections of HPF-fixed, freeze-substituted MNT-1 cells were cut on a microtome (Reichert Ultracut S; Leica) and collected on formvar-coated copper grids (75 mesh) for analysis by electron tomography. Sections were randomly labeled on the two sides with 10 nm PAG and post-stained with 2% uranyl acetate in methanol for 4 min and lead citrate for 2 min. Finally, tilt series (two perpendicular series per tomogram, angular range from −60 to 60° with a 1° increment) of 350-nm-thick sections were recorded automatically using Xplore3D (FEI Company) on a 200-kV transmission electron microscope (Tecnai 20; FEI Company) and used for reconstructing tomograms. Projection images (1,024 × 1,024 pixels) were recorded using a CCD camera (Temcam F214; Tietz Video and Image Processing Systems GmbH). After acquiring the first tilt series, the specimen grid was rotated over an angle of 90°, and a second series was recorded of the same area. Alignment of the tilt series and tomogram computing (resolution-weighted back projection) were performed using the IMOD program (Kremer et al., 1996). The 10-nm gold particles at the surface of the sections were used as fiducial markers. Manual contouring of the tomograms was performed using IMOD. Finally, the contours were meshed, and the z scale was stretched with a factor of 1.6 to correct for resin shrinkage (Mastronarde, 1997).

Image analysis and quantitation

For localization and colocalization analysis, segmentation was performed using the wavelet-based multidimensional analysis software (MIA imaging platform; Cell and Tissue Imaging Facility of Curie Institute [PICT-IBISA]; Paris, France). This segmentation algorithm is widely used to detect small, isolated structures in a heterogeneous and noisy background (Sibarita, 2005). Colocalization in Fig. 2 B was evaluated after 3D segmentation of individual channels and quantification of overlap between the two masks. Likewise, endosomal distributions (Fig. 3 C) were computed as the histogram of distances between endosomes and Golgi. Endosomes were segmented using MIA software, and their positions were detected in the x, y, and z axes. The center of the cell was manually determined as the center of Golgi labeling (GM130) along the three axes. Lastly, distances (in pixels) between each endosome position and the fixed center were calculated and reported on a graph as endosomal distribution in percent relative to distance in pixels. To determine the compaction factor (Fig. 4, D and G), >30 cells per condition were acquired, and the intensity of labeling for Tf and γ-adaptin was measured. Background fluorescence intensity was subtracted from the intensity of the whole cell (total intensity; I_t) and from within the Golgi area (I_g), and the compaction factor ($C_f = I_g/I_t$) was measured. All measures have been averaged (Fig. 4, D and G) and normalized to the control (Fig. 4 D).

For time-lapse microscopy (Fig. 6), all melanosomes were tracked after binary treatment of the original images. The intensity of the Tf-A488 signal was measured during the length of the time-lapse acquisition, within a window of 5 pixels in size, around each tracked melanosome (n = 860). Distribution of binned Tf-A488 intensities was gathered as classes of intensities. From these data, frequencies of distribution of binned Tf-A488 intensities in the vicinity of tracked melanosomes in the whole cell or within the indicated area were calculated on the whole time sequences (Fig. 6 C). Mean frame number in which individual Tf endosomes appeared in continuous contact of individual tracked melanosomes were also deduced from these data (Fig. 6 D).

Quantification of immunogold labeling on ultrathin cryosections was performed as described previously (Theos et al., 2005). The relative distribution of AP-1 in MNT-1 cells was evaluated by analyzing randomly selected cell profiles from two distinct grids directly under the electron microscope. A total of 1,526 gold particles was counted and assigned to the compartment over which they were located. The definition of the distinct compartments was based on their morphology and their previous characterization by immunogold labeling with different organelle markers (EEA-1 and Hrs for early endosomes; TGN46 for the TGN; and LAMP-1 for late endosomes/lysosomes) and internalization of endocytic tracers (BSA-gold and Tf-FITC). Tubulovesicular membranes that were located close to the trans-side of the Golgi were considered as TGN. Vacuolar endosomes were defined as electron-lucent vacuoles with no internal membranes or few internal vesicles. Multivesicular bodies were compartments delimited by a membrane with numerous internal vesicles. Electron-dense compartments with few or no internal membranes were classified as lysosomes. Clearly visible tubulovesicular membrane profiles connected to or in close association with endosomal vacuoles, melanosomes, multivesicular bodies, and lysosomes were also defined. Melanosome stages were defined by morphology (Raposo et al., 2001). Quantification of Tyrp1 distribution in control or AP-1– and KIF13A-inactivated MNT-1 cells was performed on single immunogold–labeled cryosections by counting the number of gold particles in each of the defined compartments (as for the quantification of AP-1 distribution) taken randomly in 50 cell profiles. Totals of 897, 855, and 750 gold particles were counted in control, AP-1–, and KIF13A-inactivated cells, respectively. Results are presented as a percentage of the total number of gold particles in each compartment and represent a mean and standard deviation of two independent experiments.

Online supplemental material

Fig. S1 characterizes the distribution of the endosomal recycling compartments in MNT-1 melanocytic cells using IFM analyses. Fig. S2 shows by IEM that endosomal tubules filled with Tf-biot are distinct from EEA1-positive endosomes and localize in the vicinity of pigmented melanosomes and not unpigmented premelanosomes as well as in the absence of the μ1B subunit of AP-1 in MNT-1 cells by RT-PCR. Fig. S3 illustrates by IFM the specific perinuclear clustering of recycling endosomes in KIF13A-depleted cells, the characterization by Western blotting of two different siRNAs to μ1A and KIF13A, and the immunoprecipitation of KIF13A in MNT-1 cells in the absence or presence of a blocking peptide. Fig. S4 shows the specific perinuclear clustering of recycling endosomes in cells overexpressing the tail of KIF13A or in cells microinjected with μ1A or KIF13A siRNAs. Fig. S5 shows different examples of tilt series, tomographic reconstructions, and 3D models of mature melanosomes in continuity with endosomes either filled or not with Tf-HRP. Video 1 shows dynamics of Tf-A488–filled endosomal tubules close to melanosomes by video microscopy. Videos 2–10 show a number of tilt series, tomographic reconstructions, and 3D models of pigmented melanosomes continuous with endosomal tubules. Online supplemental material is available at http://www.jcb.org/cgi/content/full/jcb.200907122/DC1.

We are grateful to S. Miserey-Lenkey and S. Lodeho for help with microinjection experiments and plasmid constructions and V. Fraisier from the Cell and Tissue Imaging Facility of Curie Institute (PICT-IBISA; Paris, France). We thank F. Jaulin and S.R.G. Setty for sharing protocols and L. Traub, M. Clague, and A.A. Peden for reagents. We are indebted to L.B. King and C. Burd for critically reading the manuscript.

This work was supported by Centre National de la Recherche Scientifique, Institut Curie, Cancéropole Ile de France, Fondation pour la Recherche Médicale (to G. Raposo), and a National Institutes of Health (NIH) grant from the National Eye Institute (R01 EY015625 to M.S. Marks). C. Delevoye is a postdoctoral fellow from the Ligue National contre le Cancer and the NIH.

Submitted: 21 July 2009
Accepted: 21 September 2009

References

Angénieux, C., V. Fraisier, B. Maître, V. Racine, N. van der Wel, D. Fricker, F. Proamer, M. Sachse, J.P. Cazenave, P. Peters, et al. 2005. The cellular pathway of CD1e in immature and maturing dendritic cells. *Traffic.* 6:286–302. doi:10.1111/j.1600-0854.2005.00272.x

Bajno, L., X.R. Peng, A.D. Schreiber, H.P. Moore, W.S. Trimble, and S. Grinstein. 2000. Focal exocytosis of VAMP3-containing vesicles at sites of phagosome formation. *J. Cell Biol.* 149:697–706. doi:10.1083/jcb.149.3.697

Bonifacino, J.S., and B.S. Glick. 2004. The mechanisms of vesicle budding and fusion. *Cell.* 116:153–166. doi:10.1016/S0092-8674(03)01079-1

Boulon, S., N. Marmier-Gourrier, B. Pradet-Balade, L. Wurth, C. Verheggen, B.E. Jády, B. Rothé, C. Pescia, M.C. Robert, T. Kiss, et al. 2008. The Hsp90 chaperone controls the biogenesis of L7Ae RNPs through conserved machinery. *J. Cell Biol.* 180:579–595. doi:10.1083/jcb.200708110

Bright, N.A., M.J. Gratian, and J.P. Luzio. 2005. Endocytic delivery to lysosomes mediated by concurrent fusion and kissing events in living cells. *Curr. Biol.* 15:360–365. doi:10.1016/j.cub.2005.01.049

Chapuy, B., R. Tikkanen, C. Mühlhausen, D. Wenzel, K. von Figura, and S. Höning. 2008. AP-1 and AP-3 mediate sorting of melanosomal and lysosomal membrane proteins into distinct post-Golgi trafficking pathways. *Traffic.* 9:1157–1172. doi:10.1111/j.1600-0854.2008.00745.x

Cox, D., D.J. Lee, B.M. Dale, J. Calafat, and S. Greenberg. 2000. A Rab11-containing rapidly recycling compartment in macrophages that promotes phagocytosis. *Proc. Natl. Acad. Sci. USA.* 97:680–685. doi:10.1073/pnas.97.2.680

Dell'Angelica, E.C. 2004. The building BLOC(k)s of lysosomes and related organelles. *Curr. Opin. Cell Biol.* 16:458–464. doi:10.1016/j.ceb.2004.05.001

Di Pietro, S.M., J.M. Falcón-Pérez, D. Tenza, S.R. Setty, M.S. Marks, G. Raposo, and E.C. Dell'Angelica. 2006. BLOC-1 interacts with BLOC-2 and the AP-3 complex to facilitate protein trafficking on endosomes. *Mol. Biol. Cell.* 17:4027–4038. doi:10.1091/mbc.E06-05-0379

Dugani, C.B., and A. Klip. 2005. Glucose transporter 4: cycling, compartments and controversies. *EMBO Rep.* 6:1137–1142. doi:10.1038/sj.embor.7400584

Fölsch, H., M. Pypaert, P. Schu, and I. Mellman. 2001. Distribution and function of AP-1 clathrin adaptor complexes in polarized epithelial cells. *J. Cell Biol.* 152:595–606. doi:10.1083/jcb.152.3.595

Gould, G.W., and J. Lippincott-Schwartz. 2009. New roles for endosomes: from vesicular carriers to multi-purpose platforms. *Nat. Rev. Mol. Cell Biol.* 10:287–292. doi:10.1038/nrm2652

Håberg, K., R. Lundmark, and S.R. Carlsson. 2008. SNX18 is an SNX9 paralog that acts as a membrane tubulator in AP-1-positive endosomal trafficking. *J. Cell Sci.* 121:1495–1505. doi:10.1242/jcs.028530

Helip-Wooley, A., W. Westbroek, H. Dorward, M. Mommaas, R.E. Boissy, W.A. Gahl, and M. Huizing. 2005. Association of the Hermansky-Pudlak syndrome type-3 protein with clathrin. *BMC Cell Biol.* 6:33. doi:10.1186/1471-2121-6-33

Hirst, J., A. Motley, K. Harasaki, S.Y. Peak Chew, and M.S. Robinson. 2003. EpsinR: an ENTH domain-containing protein that interacts with AP-1. *Mol. Biol. Cell.* 14:625–641. doi:10.1091/mbc.E02-09-0552

Hopkins, C.R., A. Gibson, M. Shipman, D.K. Strickland, and I.S. Trowbridge. 1994. In migrating fibroblasts, recycling receptors are concentrated in narrow tubules in the pericentriolar area, and then routed to the plasma membrane of the leading lamella. *J. Cell Biol.* 125:1265–1274. doi:10.1083/jcb.125.6.1265

Huizing, M., R. Sarangarajan, E. Strovel, Y. Zhao, W.A. Gahl, and R.E. Boissy. 2001. AP-3 mediates tyrosinase but not TRP-1 trafficking in human melanocytes. *Mol. Biol. Cell.* 12:2075–2085.

Huizing, M., A. Helip-Wooley, W. Westbroek, M. Gunay-Aygun, and W.A. Gahl. 2008. Disorders of lysosome-related organelle biogenesis: clinical and molecular genetics. *Annu. Rev. Genomics Hum. Genet.* 9:359–386. doi:10.1146/annurev.genom.9.081307.164303

Hurbain, I., W.J. Geerts, T. Boudier, S. Marco, A.J. Verkleij, M.S. Marks, and G. Raposo. 2008. Electron tomography of early melanosomes: implications for melanogenesis and the generation of fibrillar amyloid sheets. *Proc. Natl. Acad. Sci. USA.* 105:19726–19731.

Kremer, J.R., D.N. Mastronarde, and J.R. McIntosh. 1996. Computer visualization of three-dimensional image data using IMOD. *J. Struct. Biol.* 116:71–76. doi:10.1006/jsbi.1996.0013

Le Borgne, R., and B. Hoflack. 1997. Mannose 6-phosphate receptors regulate the formation of clathrin-coated vesicles in the TGN. *J. Cell Biol.* 137:335–345. doi:10.1083/jcb.137.2.335

Lui-Roberts, W.W., L.M. Collinson, L.J. Hewlett, G. Michaux, and D.F. Cutler. 2005. An AP-1/clathrin coat plays a novel and essential role in forming the Weibel-Palade bodies of endothelial cells. *J. Cell Biol.* 170:627–636. doi:10.1083/jcb.200503054

Manderson, A.P., J.G. Kay, L.A. Hammond, D.L. Brown, and J.L. Stow. 2007. Subcompartments of the macrophage recycling endosome direct the differential secretion of IL-6 and TNFα. *J. Cell Biol.* 178:57–69. doi:10.1083/jcb.200612131

Mastronarde, D.N. 1997. Dual-axis tomography: an approach with alignment methods that preserve resolution. *J. Struct. Biol.* 120:343–352. doi:10.1006/jsbi.1997.3919

Maxfield, F.R., and T.E. McGraw. 2004. Endocytic recycling. *Nat. Rev. Mol. Cell Biol.* 5:121–132. doi:10.1038/nrm1315

Ménager, M.M., G. Ménasché, M. Romao, P. Knapnougel, C.H. Ho, M. Garfa, G. Raposo, J. Feldmann, A. Fischer, and G. de Saint Basile. 2007. Secretory cytotoxic granule maturation and exocytosis require the effector protein hMunc13-4. *Nat. Immunol.* 8:257–267. doi:10.1038/ni1431

Meyer, C., D. Zizioli, S. Lausmann, E.L. Eskelinen, J. Hamann, P. Saftig, K. von Figura, and P. Schu. 2000. mu1A-adaptin-deficient mice: lethality, loss of AP-1 binding and rerouting of mannose 6-phosphate receptors. *EMBO J.* 19:2193–2203. doi:10.1093/emboj/19.10.2193

Nakagawa, T., M. Setou, D. Seog, K. Ogasawara, N. Dohmae, K. Takio, and N. Hirokawa. 2000. A novel motor, KIF13A, transports mannose-6-phosphate receptor to plasma membrane through direct interaction with AP-1 complex. *Cell.* 103:569–581. doi:10.1016/S0092-8674(00)00161-6

Orzech, E., L. Livshits, J. Leyt, H. Okhrimenko, V. Reich, S. Cohen, A. Weiss, N. Melamed-Book, M. Lebendiker, Y. Altschuler, and B. Aroeti. 2001. Interactions between adaptor protein-1 of the clathrin coat and microtubules via type 1a microtubule-associated proteins. *J. Biol. Chem.* 276:31340–31348. doi:10.1074/jbc.M101054200

Perret, E., A. Lakkaraju, S. Deborde, R. Schreiner, and E. Rodriguez-Boulan. 2005. Evolving endosomes: how many varieties and why? *Curr. Opin. Cell Biol.* 17:423–434. doi:10.1016/j.ceb.2005.06.008

Raposo, G., and M.S. Marks. 2007. Melanosomes—dark organelles enlighten endosomal membrane transport. *Nat. Rev. Mol. Cell Biol.* 8:786–797. doi:10.1038/nrm2258

Raposo, G., D. Tenza, D.M. Murphy, J.F. Berson, and M.S. Marks. 2001. Distinct protein sorting and localization to premelanosomes, melanosomes, and lysosomes in pigmented melanocytic cells. *J. Cell Biol.* 152:809–824. doi:10.1083/jcb.152.4.809

Roux, A., G. Cappello, J. Cartaud, J. Prost, B. Goud, and P. Bassereau. 2002. A minimal system allowing tubulation with molecular motors pulling on giant liposomes. *Proc. Natl. Acad. Sci. USA.* 99:5394–5399. doi:10.1073/pnas.082107299

Salazar, G., B. Craige, M.L. Styers, K.A. Newell-Litwa, M.M. Doucette, B.H. Wainer, J.M. Falcon-Perez, E.C. Dell'Angelica, A.A. Peden, E. Werner, and V. Faundez. 2006. BLOC-1 complex deficiency alters the targeting of adaptor protein complex-3 cargoes. *Mol. Biol. Cell.* 17:4014–4026.

Schmidt, M.R., T. Maritzen, V. Kukhtina, V.A. Higman, L. Doglio, N.N. Barak, H. Strauss, H. Oschkinat, C.G. Dotti, and V. Haucke. 2009. Regulation of endosomal membrane traffic by a Gadkin/AP-1/kinesin KIF5 complex. *Proc. Natl. Acad. Sci. USA.* doi:10.1073/pnas.0904268106.

Seiji, M., T.B. Fitzpatrick, R.T. Simpson, and M.S.C. Birbeck. 1963. Chemical composition and terminology of specialized organelles (melanosomes and melanin granules) in mammalian melanocytes. *Nature.* 197:1082–1084. doi:10.1038/1971082a0

Setty, S.R., D. Tenza, S.T. Truschel, E. Chou, E.V. Sviderskaya, A.C. Theos, M.L. Lamoreux, S.M. Di Pietro, M. Starcevic, D.C. Bennett, et al. 2007. BLOC-1 is required for cargo-specific sorting from vacuolar early endosomes toward lysosome-related organelles. *Mol. Biol. Cell.* 18:768–780. doi:10.1091/mbc.E06-12-1066

Setty, S.R., D. Tenza, E.V. Sviderskaya, D.C. Bennett, G. Raposo, and M.S. Marks. 2008. Cell-specific ATP7A transport sustains copper-dependent tyrosinase activity in melanosomes. *Nature.* 454:1142–1146. doi:10.1038/nature07163

Sibarita, J.B. 2005. Deconvolution microscopy. *Adv. Biochem. Eng. Biotechnol.* 95:201–243.

Simonsen, A., R. Lippé, S. Christoforidis, J.M. Gaullier, A. Brech, J. Callaghan, B.H. Toh, C. Murphy, M. Zerial, and H. Stenmark. 1998. EEA1 links PI(3)K function to Rab5 regulation of endosome fusion. *Nature.* 394:494–498. doi:10.1038/28879

Sitaram, A., R. Piccirillo, I. Palmisano, D.C. Harper, E.C. Dell'Angelica, M.V. Schiaffino, and M.S. Marks. 2009. Localization to mature melanosomes by virtue of cytoplasmic dileucine motifs is required for human OCA2 function. *Mol. Biol. Cell.* 20:1464–1477. doi:10.1091/mbc.E08-07-0710

Soldati, T., and M. Schliwa. 2006. Powering membrane traffic in endocytosis and recycling. *Nat. Rev. Mol. Cell Biol.* 7:897–908.

Stenmark, H. 2009. Rab GTPases as coordinators of vesicle traffic. *Nat. Rev. Mol. Cell Biol.* 10:513–525.

Theos, A.C., D. Tenza, J.A. Martina, I. Hurbain, A.A. Peden, E.V. Sviderskaya, A. Stewart, M.S. Robinson, D.C. Bennett, D.F. Cutler, et al. 2005. Functions of adaptor protein (AP)-3 and AP-1 in tyrosinase sorting from endosomes to melanosomes. *Mol. Biol. Cell.* 16:5356–5372. doi:10.1091/mbc.E05-07-0626

Theos, A.C., S.T. Truschel, D. Tenza, I. Hurbain, D.C. Harper, J.F. Berson, P.C. Thomas, G. Raposo, and M.S. Marks. 2006. A lumenal domain-dependent pathway for sorting to intralumenal vesicles of multivesicular endosomes involved in organelle morphogenesis. *Dev. Cell.* 10:343–354. doi:10.1016/j.devcel.2006.01.012

Ullrich, O., S. Reinsch, S. Urbé, M. Zerial, and R.G. Parton. 1996. Rab11 regulates recycling through the pericentriolar recycling endosome. *J. Cell Biol.* 135:913–924. doi:10.1083/jcb.135.4.913

Uzan-Gafsou, S., H. Bausinger, F. Proamer, S. Monier, D. Lipsker, J.P. Cazenave, B. Goud, H. de la Salle, D. Hanau, and J. Salamero. 2007. Rab11A controls the biogenesis of Birbeck granules by regulating Langerin recycling and stability. *Mol. Biol. Cell.* 18:3169–3179. doi:10.1091/mbc.E06-09-0779

Valencia, J.C., H. Watabe, A. Chi, F. Rouzaud, K.G. Chen, W.D. Vieira, K. Takahashi, Y. Yamaguchi, W. Berens, K. Nagashima, et al. 2006. Sorting of Pmel17 to melanosomes through the plasma membrane by AP1 and

AP2: evidence for the polarized nature of melanocytes. *J. Cell Sci.* 119:1080–1091. doi:10.1242/jcs.02804

van Ijzendoorn, S.C. 2006. Recycling endosomes. *J. Cell Sci.* 119:1679–1681. doi:10.1242/jcs.02948

Waguri, S., F. Dewitte, R. Le Borgne, Y. Rouillé, Y. Uchiyama, J.F. Dubremetz, and B. Hoflack. 2003. Visualization of TGN to endosome trafficking through fluorescently labeled MPR and AP-1 in living cells. *Mol. Biol. Cell.* 14:142–155. doi:10.1091/mbc.E02-06-0338

Wasmeier, C., M. Romao, L. Plowright, D.C. Bennett, G. Raposo, and M.C. Seabra. 2006. Rab38 and Rab32 control post-Golgi trafficking of melanogenic enzymes. *J. Cell Biol.* 175:271–281. doi:10.1083/jcb.200606050

Wei, M.L. 2006. Hermansky-Pudlak syndrome: a disease of protein trafficking and organelle function. *Pigment Cell Res.* 19:19–42. doi:10.1111/j.1600-0749.2005.00289.x

Wilcke, M., L. Johannes, T. Galli, V. Mayau, B. Goud, and J. Salamero. 2000. Rab11 regulates the compartmentalization of early endosomes required for efficient transport from early endosomes to the trans-Golgi network. *J. Cell Biol.* 151:1207–1220. doi:10.1083/jcb.151.6.1207